CARDIFF UNIVERSITY
PRIFYSGOL CAERDYDD

ORCA – Online Research @ Cardiff

This is an Open Access document downloaded from ORCA, Cardiff University's institutional repository:https://orca.cardiff.ac.uk/id/eprint/150241/

This is the author's version of a work that was submitted to / accepted for publication.

Citation for final published version:

Sun, Qiliang, Alves, Tiago M. , Wu, Shiguo, Zhao, Minghui and Xie, Xinong 2023. Early Miocene magmatism in the Baiyun Sag (South China Sea): A view to the origin of intense post-rift magmatism. Gondwana Research 120 , pp. 127-144. 10.1016/j.gr.2022.05.013

Publishers page: http://dx.doi.org/10.1016/j.gr.2022.05.013

Please note:
Changes made as a result of publishing processes such as copy-editing, formatting and page numbers may not be reflected in this version. For the definitive version of this publication, please refer to the published source. You are advised to consult the publisher's version if you wish to cite this paper.

This version is being made available in accordance with publisher policies. See http://orca.cf.ac.uk/policies.html for usage policies. Copyright and moral rights for publications made available in ORCA are retained by the copyright holders.

Early Miocene magmatism in the Baiyun Sag (South China Sea): A view to the origin of intense post-rift magmatism

Qiliang Sun[1, 2,*], Tiago M. Alves[3], Shiguo Wu[4], Minghui Zhao[5], Xinong Xie[1]

[1]Hubei Key Laboratory of Marine Geological Resources, China University of Geosciences, Wuhan 430074, China;
[2]Laboratory for Marine Mineral Resources, Qingdao National Laboratory for Marine Science and Technology, Qingdao 266061, China;
[3]3D Seismic Lab, School of Earth and Environmental Sciences, Cardiff University, Main Building, Park Place, Cardiff CF10 3AT, UK;
[4]Laboratory of Marine Geophysics and Georesources, Institute of Deep-sea Science and Engineering, Chinese Academy of Sciences, Sanya 572000, China;
[5]Key Laboratory of Ocean and Marginal Sea Geology, South China Sea Institute of Oceanology, Chinese Academy of Sciences, Guangzhou 510301, China
Corresponding author: Qiliang Sun (sunqiliang@cug.edu.cn)

Abstract:

Post-rift magmatism associated with seafloor spreading (~32.0 Ma to ~15.5 Ma) and post-spreading tectonics (from ~15.5 Ma to the present day) is widely recorded in the South China Sea (SCS). However, the phenomena originating this magmatism are still under debate, hindering a full understanding of the SCS' evolution. In this study, extensive and voluminous magmatic bodies in the northern SCS are investigated based on the integration of 3D/2D seismic and borehole data. Magmatism occurred from ~19.0 Ma to ~17.5 Ma, a period of time marking the cessation of seafloor spreading, above listric boundary faults formed on the southern shoulder of the Baiyun Sag. Magmatism close to the main basin depocentre (Magmatic Zone 1) is documented in the form of oblique/saucer sills that step upwards. They have fed volcanoes and lava flows to a paleo-seabed via igneous dikes. In contrast, magmatism in the shoulders of the Baiyun Sag (Magmatic zones 2 and 3) occurred above listric boundary faults that formed large magma pathways. The phase of magmatism documented in this work was probably triggered by the retreat of the Hainan Plume and associated mantle readjustments during jumps in spreading-ridge location. These events rejuvenated mantle upwelling underneath the highly stretched Baiyun Sag to generate partial melting. Mantle upwelling also reactivated the listric boundary faults flanking this basin, generating migration pathways for deep-seated magma. This work addresses the syn-spreading magma plumbing system of the Baiyun Sag in detail, and provides evidence for the origin of intense post-rift magmatism in the northern SCS. It also highlights that mantle readjustments triggered by changes in seafloor spreading (ridge jump or cessation of spreading) can generate significant post-rift magmatism.

Keywords: Magmatism; volcanoes; sills; magma plumbing system; listric boundary fault; Hainan Plume; South China Sea.

1. Introduction

The SCS is located between the Eurasian, Pacific and India-Australia plates, having experienced a complex history of seafloor spreading, associated tectonic subsidence, plate collision and strike-slip tectonics, making it as an ideal location to explore Earth Systems as a whole (Fig. 1). The SCS is considered as a magma-poor to intermediate continental margin because it has limited syn-rift magmatism (lack of seaward-dipping reflections) in its deep-water, continental-breakup regions (Clift et al., 2001; Yan et al., 2006; Ding et al., 2013; Franke, 2013; Sun et al., 2019a). Nevertheless, post-rift magmatism is frequently observed in oceanic basins and continental margins surrounding the SCS (Li and Rao, 1994; Zou et al., 1995; Yan et al., 2006; Wang et al., 2012; Li et al., 2014; Zhao et al., 2014; Fan et al., 2017; Ding et al., 2018; Larsen et al., 2018; Ma et al., 2018; Sun et al., 2020a). It is recognized in the literature as comprising two distinct phases: *syn-spreading* (~32 Ma to 15.5 Ma) and *post-spreading* (15.5 Ma to the present day).

Syn-spreading magmatism occurred in the SCS near the end of the seafloor spreading stage (Zhao et al., 2016; Deng et al., 2018; Sun et al., 2020c). This phase of magmatism provided important clues on how the mantle and lithosphere adjust to changes in mantle convection and geographic changes in the position of the spreading centres per se (Zou et al., 1995; Zhao et al., 2014, 2016; Deng et al., 2018; Ma et al., 2018; Sun et al., 2014a, 2020c). However, fundamental questions about the age, volume, contributing plumbing systems, and origin of syn-spreading magma are still unresolved. This inhibits our understanding of the regional magmatic plumbing system and evolution of the SCS.

This study addresses the extensive and voluminous magmatism recorded around the southern shoulder of the Baiyun Sag using an integrated 3D seismic volume (~9800 km^2), a ~6100 km 2D seismic dataset, and information from two exploration wells. It aims to: (1) systematically characterize the geometry and distribution of this focused magmatism, (2) date the magmatism and calculate its total volume in the Baiyun Sag, (3) address the main factors controlling the plumbing system that fed the interpreted magmatic features, and (4) explore the probable origins of magma in a post-rift northern SCS.

2. Geological setting

2.1. Evolution of the northern margin of the SCS

The SCS is a tectonically complex region located between the Eurasian, Pacific and India-Australia plates, being divided into east, northwest and southwest sub-basins (Fig. 1) (Briais et al., 1993; Frank et al., 2014). Rifting of an Andean-type continental margin during the latest Cretaceous and early Paleocene initially opened the SCS (Ru and Pigott, 1986). Following continental rifting, continental breakup and seafloor spreading occurred during the early Oligocene (~33 Ma) in the East and Northwest Sub-basins, with the spreading ridge subsequently jumping southwards to the Southwest Sub-basin at ~23.6 Ma (Li et al., 2014; Zhao et al., 2016). Seafloor spreading finally terminated in the East Subbasin at ~15 Ma, and in the southwest Sub-basin at ~16 Ma (Li et al., 2014).

Three main tectonic events, Zhuqiong, Nanhai and Dongsha, mark the evolution of the SCS (Gong and Li, 1997; Pang et al., 2008) (Fig. 2). The Zhuqiong Event (Paleocene - Eocene) coincides with the continental rifting stage, and two peaks (marked with red lines in Fig. 2) correlate with two main extensional episodes in the Pearl River Mouth Basin (Gong and Li, 1997). The Nanhai Event (~32-15 Ma) reflects the initial opening, ridge jump and maximum extension events of the SCS, which correlate with three periods of normal faulting: 32-29 Ma, 23.8-21.0

Ma, and 18.5-16.5 Ma (Deng et al., 2019). The younger Dongsha Event records widespread faulting, tectonic uplift and magmatism in and around the Dongsha Massif after ~10 Ma (Lüdmann and Wong, 1999).

The Pearl River Mouth Basin, the focus of this work, is one of many offshore basins located along the northern SCS formed by continental rifting (Pang et al., 2008). It comprises multiple sub-basins, or sags, with the Baiyun Sag comprising the deepest and broadest sag with an area of 2×10^4 km^2 (Gong and Li, 1997). The Baiyun Sag is a half-graben basin bounded by landward-dipping listric boundary faults to the south - also named *detachment faults* in the literature (Pang et al., 2008; Yang et al., 2018; Zhou et al., 2018; Fang et al., 2022) (Fig. 3). These listric boundary faults sole out in the upper mantle, probably at the Moho, which is shown as a series of semi-continuous, linear, high-amplitude reflections in seismic data (Lei et al., 2018; Pang et al., 2018; Yang et al., 2018; Zhao et al., 2018a; Zhou et al., 2018). The Baiyun Sag is filled by a sedimentary succession exceeding 17 km in thickness (Fig. 3), and comprises several hydrocarbon fields (Pang et al., 2008). The crust of the Baiyun Sag was highly stretched during continental rifting; stretching factors (β) reach 4.0 (Chen, 2014), while crustal thickness can be less than 7.0 km in places (Huang et al., 2005). Evolution models explain this thin, stretched crust as resulting from lower crustal flow (Clift et al., 2002) or magma-assisted rheologically weakening (Chen, 2014).

2.2. Magmatism in the northern SCS

The SCS is a magma-poor to intermediate continental margin due to the lack of seaward-dipping reflections (SDRs) and the low volumes of rift-related igneous rocks encountered there (Clift et al., 2001; Yan et al., 2006; Ding et al., 2013; Franke, 2013; Li et al., 2019). Nevertheless, recent studies have identified voluminous laccoliths and sills on the sediment-rich distal margin (Sun et al., 2019b; Zhang et al., 2021). Magmatism during the main continental-rifting phase (between 64 Ma and 32 Ma) had a bimodal character on the continental shelf and South China block (Yan et al., 2006; Zhao et al., 2016). Magma emplacement thus started during the continental rifting stage, propagated seaward, and lasted until the early post-rift stage (>23.8 Ma; Zhang et al., 2021).

During the syn-spreading, or continental breakup stage, magmatism occurred in the SCS spreading centre and typically formed new ocean crust (Ding et al., 2018; Larsen et al., 2018). It also affected the northern continental slope of the SCS in the form of magma extruded onto a shallow seafloor or land (Li and Rao, 1994; Zou et al., 1995; Yan et al., 2006; Wang et al., 2012; Zhao et al., 2014, 2016; Fan et al., 2017; Ma et al., 2018; Sun et al., 2020c). Well BY7-1 drilled through these extruded magmatic edifices to reveal basalt and tuffs with a lower Miocene age (17.1 ± 2.5 Ma) based on K-Ar dating (Li and Liang, 1994; Yan et al., 2006). This age agrees with the local seismic stratigraphy (Zhao et al., 2016; Ma et al., 2018; Sun et al., 2020c). Some shallow magma intrusions are also identified as sill complexes in the Baiyun Sag (Sun et al., 2014a). Normal faults likely provided the main pathways for the magma intruding these shallow sedimentary units (Deng et al., 2018; Sun et al., 2020c).

Post-spreading magmatism in the northern SCS is mainly characterized by volcanoes and lava flows, being widely observed in the oceanic basin, on the modern continental slope, and also onshore (Xu et al., 2012; Li et al., 2014; Yan et al., 2016; Sibuet et al., 2016; Ding et al., 2018; Zhao et al., 2018b; Sun et al., 2020a, b). Igneous bodies and edifices are composed of alkali basalts with subordinate tholeiites, revealing basaltic oceanic-island type characteristics (Yan et al., 2018; Wang et al., 2012; Zhang et al., 2017). Close to the continent-ocean transition, magmatism occurred above the largest planar and listric boundary faults, suggesting these structures formed magma pathways (Fan et al.,

2017; Sun et al., 2020b).

The sources, or driving forces, of magmatism in the northern SCS are still under debate. Lester et al. (2014) have proposed that the convective removal of continental lithosphere between the terminal phases of continental rifting (latest Eocene) and the post-rift spreading stage (early Miocene) was able to generate widespread magmatism in the northern SCS. The Hainan Plume possibly fed this post-spreading magmatism (e.g. Franke, 2013; Xia et al., 2016, 2018; Fan et al., 2017). Moreover, extension caused by thermal cooling and subsidence of the oceanic/attenuated continental lithosphere may have also contributed to post-rifting magmatism (Song et al., 2017). The youngest magma (<8.2 Ma) in the northeastern SCS was probably emplaced during the Dongsha Event in association with tectonic collision between Taiwan and the Luzon Arc (Sun et al., 2020b).

3. Data and methods

An integrated 3D seismic dataset covering an area of ~9800 km^2, a 2D seismic dataset comprising ~6100 km, and two exploration wells, are used in this study. The 3D seismic-reflection data were acquired from 2000 to 2016 using 3000 m long streamers comprising 240 channels, and bin sizes of 12.5 m or 12.5 × 25.0 m. Regional 2D seismic reflection data were acquired from 1996 to 2008 with 1200-2400 m long streamers comprising 128 channels, and a bin size of 12.5 m. The seismic reflection data are time-migrated and zero-phase processed. They are displayed using SEG's (Society of Exploration Geophysicists) normal polarity whereby a downward increase in acoustic impedance corresponds to a positive red reflection on seismic profiles (Brown, 2004). The interpreted magmatic bodies occur at a depth between ~2 s two-way time (twt) and ~6 s twt, where the frequency of the seismic data (2D and 3D) ranges from 45 Hz to 25 Hz. The extrusive body drilled by well BY7-1 has an interval velocity of ~4500 m/s, being surrounded by strata with a p-wave (Vp) velocity of 2800 m/s (Sun et al., 2020c). Consequently, the minimum vertical resolutions of extrusive bodies are ~25 m at a shallow depth of ~2 s (twt) and ~45 m at a depth of ~6 s (twt).

Mounded edifices in the study area are onlapped by younger sediment and show positive-amplitude reflections on their tops (Figs. 6-7, 11-12). Internal reflections are sub-parallel, downward-curved and convergent (Figs. 7, 11-12), similar to the seismic character of recognized volcanoes (Magee et al., 2013; Zhao et al., 2014; Reynolds et al., 2018; Niyazi et al., 2021a). One mounded structure was drilled by exploration well BY7-1, which found basalt and tuffs (Qin, 2000; Zhao et al., 2016; Ma et al., 2018; Sun et al., 2020c). Therefore, mounded edifices are interpreted as volcanoes that are isolated or merged to form volcanic complexes (Figs. 6, 10). In parallel, layered high-amplitude seismic reflections, interpreted as lava flows, extend for long distances on the paleo-seafloor and are, in places, related to the volcanic edifices (Fig. 6).

Saucer/sheeted/oblique positive seismic anomalies underlie the volcanoes and are linked to the latter through near-vertical diffractive zones and faults (Figs. 6-7). Some are concordant, but most diffractive zones cross-cut the adjacent strata (Figs. 6-7, 9d, 10). This is a character akin to the 'typical' magmatic sills documented in Smallwood and Maresh (2002), Thomson and Hutton (20040 and Alves et al. (2015) and, thus, are interpreted as such. Accordingly, near-vertical diffractive zones connected to the sills and overlying volcanoes comprise igneous dikes (Figs. 6-7). Intrusions (sills, dikes) have not been drilled by exploration wells in the study area, but should comprise rocks with a p-wave velocity of ~7000 m/s based on sonic-logs data from the North Sea (Berndt et al., 2000). Therefore, seismically resolved sills have thicknesses of more than 39 m in shallow strata, and 70 m in deep strata.

Biostratigraphic, P-wave velocity, Gamma

Ray (GR) and lithological data were gathered from exploration wells BY7-1 and L9, and later used to produce a synthetic seismogram and correlate key seismic horizons to known seismic-stratigraphic units (Fig. 4). The ages of regional seismic-stratigraphic markers were also considered from previous studies (Gong and Li, 1997; Pang et al., 2008; Deng et al., 2018). These include seven regional seismic horizons: the Seafloor, T10 (~5.0 Ma), T20 (~10.5 Ma), T40 (~15.5 Ma), T60 (~23.8 Ma), T70 (~32.0 Ma) and Tg (Fig. 5). Three other reference horizons were mapped: TRa (~17.5 Ma), TRb (~18.5 Ma) and TRc (~19.5 Ma) (Figs. 6-12), together with the tops/bases of local mounded edifices (Fig. 9).

The ages of extrusive features were constrained by the lowermost seismic reflection onlapping the extrusive features (Trude et al., 2003). The thickness of magmatic bodies was calculated by subtracting the converted depths of their tops and bases (Figs. 9a-c). Variance slices were also used to better delineate the magmatic bodies in the study area (Figs. 8a, 12a). Variance maps, or slices, compare the similarity of adjacent seismic trace and thus clearly delineate the boundaries of depositional and tectonic structures, e.g. faults, volcanoes and channels (Brown, 2004).

4. Results and interpretations

4.1. Deep-seated structures in the Baiyun Sag

Two megasequences, syn-rift and post-rift, are identified in this work. They are separated by horizon T70, a continuous, positive seismic reflector (Fig. 5). The base of the syn-rift megasequence coincides with horizon Tg, a discontinuous high-amplitude seismic reflection (Fig. 5). In the study area, the syn-rift megasequence fills a half-graben basin bounded to the south by a listric boundary fault. Strata in the half graben are semi-continuous with sub-parallel, and occasional chaotic, seismic reflections (Fig. 5). Seismic reflections are mostly chaotic below horizon Tg; however, a series of semi-continuous, linear, high-amplitude seismic reflections can still be recognized (Fig. 5). They are contorted and gently uplifted below the Baiyun Sag (Fig. 5), and interpreted as the Moho reflector separating the crust from the mantle following Pang et al. (2018), Yang et al. (2018); Zhao et al. (2018a) and Zhou et al. (2018). Listric boundary faults offsetting the lower crust are also observed and usually terminate (sole out) near the Moho.

The lower part of the post-rift sequence shows well-stratified, medium- to high- amplitude seismic reflections (Fig. 5). Enhanced seismic anomalies and mounded structures observed within them (see details in the following section) are often located above listric boundary faults (Fig. 5). The upper part of the post-rift megasequence is characterized by its chaotic to progradational seismic reflections, especially on the middle to upper continental slope (Fig. 5). Several normal faults are observed in this post-rift megasequence (Fig. 5).

4.2. Character of post-rift magmatism

Extrusive (volcanoes and lava flows) and intrusive (saucer, oblique and sheeted sills) features are widely identified in lower Miocene strata along the southern shoulder of the Baiyun Sag (Figs. 6-12). According to their size, volume, and seismic character, three magmatic zones (MZ1, MZ2 and MZ3) are identified in this work (Fig. 3).

4.2.1. Magmatic Zone 1 (MZ1)

MZ1 is located on the southeastern shoulder of the Baiyun Sag, where sediment thickness is >17 km. It has a NE-SW strike parallel to the main sag (Fig. 3). A total of 41 seismic-scale volcanoes/lava flows are identified in MZ1 (Fig. 13a; Table S1). Most volcanoes are conical (e.g. V20 and V21) but a few have flat tops (e.g. V18 in Fig. 7). Normal faults and local folds occur directly above the tops of volcanoes (Figs. 6-7). They indicate these faults to post-date the volcanoes and probably relate to differential compaction between ‘hard’ magmatic rock and

surrounding 'soft' sediments (Schofield et al., 2017; Sun et al., 2020c). An isolated volcano (e.g. V20) is connected to a nearby volcano V21 through layered lava flows, forming a volcanic complex (Fig. 7). The lava flow extends for more than 25 km and spans an area of ~72 km^2 (Table S1). In MZ1, volcanoes occur in an area ranging between 1 km^2 and 78 km^2 for an average of 11.53 km^2. Their height ranges from 56 m to 844 m, for an average of 447 m (Fig. 13f). Their thickness varies from 43 m to 473 m, for an average of 258 m (Figs. 13c-d). They have a total volume of 125.26 km^3 and an average volume of 5.01 km^3 (Fig. 13b). The flanks of volcanoes are generally gentle with an average dip of 19.7° (Table S1).

Volcanoes V8 and V9 are directly located over the lava flows, suggesting these latter are slightly older than the volcanoes that overlie it (Fig. 6). These lava flows are offset by several normal faults, but their thickness remains constant on hanging-wall and footwall blocks (Fig. 6). This indicates that faults post-date the lava flows. The relationships between different volcanoes also reflect their emplacement ages; for example, a continuous seismic horizon separates V18 from the overlying V20-V22, indicating that V18 is older than the volcanic complex formed by V20-V22 (Fig. 7).

Seismic reflections onlapping the volcanoes reveal that horizon TRa (17.5 Ma) drapes all edifices in MZ1. Moreover, the lowermost onlapping seismic reflections of most volcanoes in MZ1 occur between horizons TRa and TRb (18.5 Ma). Some volcanoes are directly onlapped by TRb (Figs. 6-7, 9). The oldest extrusive edifices (V18, L1 and L2) are considered as 19.5 Ma old because they are directly draped by horizon TRc (Figs. 6-7). In general, onlapping seismic reflections indicate that erupted events in MZ1 lasted for ~1.5 Ma, from 19.0 Ma to ~17.5 Ma (Figs. 6-8).

The most striking observation in MZ1 is the presence of intrusive sill swarms. About 126 seismic-scale sills are identified under the volcanoes and lava flows. The total volume of these sills is 66.52 km^3, for an average volume of 0.53 km^3 (Fig. 13b). Most sills cross-cut sedimentary units and obliquely step upward (Figs. 6a-b). Some sills are linked to form sill complexes (S121, Fig. 8b), especially those intruding close to the paleo-seabed (Sun et al., 2014a). These sills are mainly saucer-shaped, while the overlying sills (sills in the upper level) mostly originate from the tips of the deeper sills (sills in the lower level) (Fig. 8c-d). Some sills are offset by normal faults, but their thickness is constant across these structures (Figs. 6a-b, 7), indicating that faults were developed after the emplacement of the sills. Near-vertical zones of disruption link the sill swarms with overlying (extrusive) edifices (Figs. 6-7). Therefore, the vertical dikes - together with the obliquely-stepped sills - likely comprised the main migration pathways for magma in MZ1.

No wells drilled through the sills and, thus, the precise ages for sill intrusion cannot be confirmed. Some sills deformed the sediment above (e.g., forced fold S121) and their ages can only be estimated by their oldest onlapping seismic reflections. There are no forced folds above most of the sills interpreted in MZ1. Considering the sills fed the interpreted volcanoes and lava flows, their ages are probably the same to or a bit older than these same volcanoes and lava flows, e.g. spanning 19.0 Ma to 17.5 Ma (Table S1).

4.2.2. Magmatic Zone 2 (MZ2)

MZ2 is observed to the southeast of MZ1 and coincides with a small-scale structural high (Fig. 3). A listric boundary fault cuts through MZ2 as shown on 2D seismic profiles, but only its northwest part is imaged in 3D seismic data (Fig. 3). Compared to MZ1, Magmatic Zone 2 shows a large-scale volcanic complex composed of 12 volcano edifices and associated lava flows. The volcanic complex in MZ2 covers an area of ~1152 km^2 for an average thickness of ~835 m and a volume of ~961.9 km^3 (Table S1).

The tops of imaged volcanos are very rugged and show a continuous, positive seismic reflection. The height of volcano edifices ranges from 191 m to 2768 m (Table S1), a value that increases towards the middle of the volcanic complex (Fig. 10). Some volcanoes occur just below the modern seafloor. The volcanic complex is totally onlapped by younger strata, with the oldest onlapping reflections correlating with horizon TRb (18.5 Ma). Overlying strata, especially those directly covering the volcano edifices, are folded due to differential compaction (Schofield et al., 2017; Sun et al., 2020c) (Figs. 10).

The base of the volcanic complex is rugged and gradually uplifted ('pulled-up') towards its middle part (Fig. 10). Its interior shows moderate- to high-amplitude seismic reflections, but chaotic in places. Low-amplitude patches within the volcano edifices are also observed. Strata underlying the volcanic complex are not well imaged because of losses in the seismic signal (Reynolds et al., 2017), or were disrupted by the vertical migration of magma (Fig. 10). Nevertheless, large-scale saucer sills (30 sills) are still identified in the strata underlying the volcanoes (Fig. 10). They have an average thickness of 123 m, ranging between 81 m and 357 m, and a total volume of 6.84 km^3. Linear and oblique (discordant) sills are seldom observed in MZ2. Only three saucer sills are associated with forced folds - all dated as 18.5 Ma. Considering that the eruptive events in MZ2 are mainly focused near the 18.5 Ma seismic marker, underlying sills should have been emplaced during this same magmatic event.

Mounded edifices originating from the basement are characterized by their low-amplitude, chaotic seismic reflections (Fig. 10). Their bases cannot be identified in seismic data, but their tops are marked by sub-continuous, high-amplitude seismic reflections. Because they originated from the basement, and are onlapped by strata older than T60, we interpret them as syn-rift volcanoes or basement highs. These syn-rift volcano edifices terminate directly below the middle of the volcanic complex in MZ2 (Figs. 10).

4.2.3. Magmatic Zone 3 (MZ3)

MZ3 coincides with the southern shoulder of the Baiyun Sag and shows a E-W orientation (Fig. 3). Similarly to MZ2, listric boundary faults propagate through MZ3 (Fig. 3). MZ3 is characterized by its extrusive magma edifices, such as volcanoes and lava flows (Figs. 11-12), forming eight (8) volcanic complexes (Table S1). In general, there are 76 seismic-scale volcano edifices in MZ3; they are generally smaller than those in MZ2 and have heights ranging from 74 m to 700 m (though most are less than 300 m), for an average height of 247 m (Fig. 13f; Table S1). These extrusive edifices cover a total area of 561.8 km^2, for a total volume of 89.8 km^3, a value much smaller than the volume of magma erupted in MZ2 (~961.9 km^3) (Fig. 13b). The flanks of volcanoes in MZ3 are also gentle, with gradients ranging from 5.3° to 30.3°, for an average value of 17.5° (Table S1). The top of extrusive edifices show continuous, positive seismic reflections (Figs. 11). Their bases also reveal continuous, positive seismic reflections (Figs. 11, 12c-d). Internal reflections in the volcanoes have low amplitude, though layered intervals can also occur.

The most important observation in MZ3 is the close relationship between volcanoes and normal faults; nearly all the volcanoes are located near the upper tips of normal faults. The thickness of erupted materials on the hanging-wall blocks of these faults is significantly larger than that on the immediate footwalls where normal faults propagated to offset the volcanoes above (Figs. 11a-b). This last observation suggests that the normal faults served as magma conduits (Sun et al., 2020c). The strata overlying the conical volcanoes are also gently folded and faulted due to differential compaction (Sun et al., 2020c).

Volcanoes in MZ3 are slightly younger than in MZ1 and MZ2. Nearly all volcanoes were

extruded at the level of horizon TRa (17.5 Ma), with only one small volcano observed at horizon T30 (~13.8 Ma) (Table S1). Sills are not particularly well developed in MZ3 and only 18 saucer/oblique sills are identified in seismic data. Their thickness range from 67 m to 144 m, for an average value of 95 m (Figs. 13c-d; Table S1). The total volume of these sills is 3.87 km^3. Forced folds, and the close relationship with overlying volcanoes, indicate that sills were also emplaced at 17.5 Ma.

5. Discussion

This study documents a large volume of magma, at least 1263.7 km^3, erupted on the southern shoulder of the Baiyun Sag in a very short period of time (~1.5 Ma). Considering the resolution of our seismic data (e.g. Fig. 10), more magmatic bodies should occur in the deeper successions that are less acoustically resolved (Zhang et al., 2021). Though magmatic edifices have been reported in previous studies (Sun et al., 2014a, 2020c; Zhao et al., 2014, 2016; Deng et al., 2018; Ma et al., 2018), key questions such as the origin of such edifices, and the location of the plumbing systems feeding the magma to the Baiyun Sag, have yet to be fully addressed.

5.1. Magma emplacement systems in the Baiyun Sag

Magmatism varied spatially and temporally across the study area (Figs. 6-12). MZ1 shows a large number of intrusions and small-scale extrusions spanning in age from 19.0 Ma to 17.5 Ma (Table S1), whilst MZ2 comprises large-scale extrusions that occurred at ~18.5 Ma (Fig. 10). Extrusive edifices were also identified in MZ3; they are small when compared to MZ2 (Table S1). In general, intense early Miocene magmatism occurred along the southern shoulder of the Baiyun Sag where deep-seated boundary faults are observed (Fig. 14). These faults penetrated downward to, and extended along, the Moho (Zhao et al., 2018a; Yang et al., 2018). They worked as weak zones in the thinnes continental crust and were reactivated during the early Miocene (Deng et al., 2018). This promoted the generation of magma pathways linking deep-seated sources to shallow intrusions and volcanoes as proven by: (1) the spatial coincidence between magmatism and listric boundary faults (Figs. 3-4), and (2) the fact that ~83% of the total measurable magma volume occurs directly above the listric boundary faults (Figs. 10-12). Interconnected sills, dikes (mainly in MZ1) and normal faults (especially in MZ3) served as the main magma migration pathways (Figs. 6-8 and 11).

This work proposes that the early Miocene magma plumbing system in the Baiyun Sag evolved as a series of discrete stages. First, melting magma migrated upward along listric boundary faults (Fig. 14). In the main depocentre, magma leaked out from listric boundary faults and intruded the sedimentary units above. This magma intruded at an oblique angle with the stratigraphy and fed the volcanoes/lava flows reaching the surface through dikes (Fig. 14). These phenomena generated a large number of magma intrusions in the sedimentary sequences imaged in seismic data, plus small-scale extrusions on successive paleo-seafloors, forming the magmatic features interpreted in MZ1 (Figs. 6, 14). In MZ2, a large volume of magma migrated upward along the listric boundary faults, erupting in the early Miocene to form a volcanic complex (Fig. 10). Because MZ2 is directly located above the main magma migration pathways (listric boundary faults), it is marked by its voluminous extrusions (Figs. 10, 14) rather than by the multiple intrusions documented in MZ1 (Fig. 6). In general, MZ1 is closer to the main depocentre of the Baiyun Sag and, consequently, also closer to the main source of magma. Therefore, magmatism in MZ1 (~19.0 Ma) started a bit earlier than in MZ2 (18.5 Ma), which is located to the south of main basin depocentre (Fig. 3 and Table S1). This agrees with the assumption that the magma needed more

time to reach the upper tips of listric boundary faults in MZ1 because of the longer migration distances recorded here.

The westernmost depocentre (MZ3) records the longest distance to the magma source, and thus magmatism is the youngest amongst the three Magmatic Zones (~0.5 Ma younger than in MZ2). Moreover, magmatism in MZ3 is directly located above listric boundary faults, and other normal faults offsetting the strata are more widely distributed than in Magmatic Zones 1 and 2 (Figs. 3, 11-12). MZ3 is dominated by extrusive edifices and lava flows, and normal faults served once again as the main magma migration pathways (Figs. 11-12).

The observations above suggest that both the listric boundary faults and the thickness of strata in the Baiyun Sag had a key role in controlling the number and volume of magma extrusions (and intrusions) in MZ1 to MZ3 (Fig. 13). Extrusive lava in MZ2 and MZ3 was able to accumulate above listric boundary faults (Figs. 10-12), whilst lava in MZ1 intruded into thick sedimentary sequences (Figs. 6-7). Deep-seated magmatic pressure is usually high, facilitating the vertical migration of magma along weak zones such as basin-bounding faults (Rohrman, 2013). This results in the final eruption of magma onto the paleo-seabed to form the extrusive edifices interpreted in this study (Figs. 10-12). Thick sedimentary sequences, when present, may generate high overburden pressures, which deviate the sub-vertical propagation of magma and favor the formation of sill-dominated igneous plumbing systems, e.g., offshore Otway Basin (Niyazi et al. 2021b) and the Qiongdongnan Basin (Sun et al., 2022). The thickness of strata and the relative size of intrusions thus influence the shapes of sills and the generation of associated folds above them. Large-scale, lens-shaped sill complexes usually occur at shallow depths, close to the seabed, and forced folds develop above them (Sun et al., 2014) (Fig. 8).

Although saucer sills can be observed at variable depths below the seafloor, they predominate in MZ2 and MZ3 within thin stratigraphic successions (Figs. 10-11), with the large-scale sills in MZ2 showing forced folds above them (Table S1). Oblique and sheeted sills mainly developed in thick sedimentary sequences and did not promote the formation of overlying forced folds. Only five forced folds are observed above the latter sequences (Table S1).

5.2. Mechanisms explaining the origin of post-rift magma in the Baiyun Sag

The widespread magmatism revealed in the Baiyun Sag occurred during a tectonic quiescent period, i.e. between a ridge jump event at 23.8 Ma (Li et al., 2014) and intense tectonic activity associated with the Dongsha Event (<10 Ma) (Lüdmann and Wong, 1999). Therefore, it is not directly related to regional tectonic events. The restricted time interval (~1.5 Ma) in which this magmatism occurred is another aspect that needs to be addressed (Table S1).

Normal faulting is recorded in the Baiyun Sag during the early Miocene (18.5-16.5 Ma), and included the reactivation of basin-shoulder faults – the listric boundary faults interpreted in this work (Sun et al., 2014b; Deng et al., 2018). This character suggests the Baiyun Sag was under the effect of an extensional stress regime at this time, which was responsible for the faulting and magmatism - resulting from mantle upwelling and decompression melting - identified in seismic data. However, considering the nature of the voluminous (Fig. 13) and short-lived magmatism in the study area (Table S1), this same magmatic event was probably not caused by a slow, long-lived extensional process, such as that recorded during the thermal cooling and subsidence of oceanic and stretched continental lithosphere, and assumed to be have been responsible for most volcanism in the oceanic basins of the SCS (Song et al., 2018).

Widespread oceanic-island-basalt (OIB) magmatic rocks (e.g. Yu et al., 2018; Yan et al., 2018) and recent teleseismic images (Xia et al.,

2016) suggest the presence of a mantle plume (Hainan Plume) around the Hainan Island. Geochemical evidence has also shown that seafloor spreading in the SCS was geologically linked to this mantle plume (Xu et al., 2012; Yan et al., 2014). Considering the character of the magmatic event in this work, short-lived and with an abrupt ending, and its relative location between the Hainan Island and SCS's spreading centre (Fig. 1a), mantle plume retreat is the most plausible model explaining its origin. As seafloor spreading occurred by lithospheric breakup (Fig. 15a), a ridge suction effect may have contributed to the obduction of the mantle plume moving it out of the spreading centre (Xu et al., 2012; Huang et al., 2020) (Fig. 15b). At ~23.8 Ma, the southwest jump of the SCS' spreading ridge - from the East Sub-basin to the Southwest Sub-basin - greatly changed the regional mantle-convection patterns, i.e., convection velocity and strength (Huang et al., 2020), triggering the decoupling between the Hainan Plume and the spreading centre in the East Sub-basin. In such a setting, the Hainan Plume gradually retreated towards the north Hainan Island, where it is located at present (Figs. 1c, 15c).

Approximately 5 Ma after the spreading centre jump (at ~19 Ma b.p), the head of the Hainan Plume retreated to a highly-stretched Baiyun Sag recording stretching factors (β) of 4 with a crust ~7 km thick (Huang et al., 2005; Chen, 2014). This facilitated mantle upwelling and the partial melting of magma, generating the magmatic features interpreted in this work (Fig. 15c). The presence of a thermal anomaly in the study area is confirmed by the sudden decrease in thermal subsidence in the central Baiyun Sag at around 17-18 Ma (Xie et al., 2014). Mantle upwelling was then able to reactivate the listric boundary faults mapped in this work. After another 1.5 Ma, the head of the mantle plume retreated further northwest, away from the Baiyun Sag, and magmatism terminated after 17.5 Ma - agreeing with the observations in this study. The extensive and voluminous magmatism occurred in such a short period of time confirms the character of mantle-plume magmatism reported in previous work (e.g. White and McKenzie, 1989; Menzies et al., 1993; Li et al., 2022).

Our hypothesis predicts that relatively weaker magmatism occurred on the northern SCS shelf during the retreat of the Hainan Plume because the thick continental crust inhibited it. This argument is supported by the lack of post-spreading magmatism on the continental shelf. However, we must note that the model proposed in this work still has some limitations. For example, the mechanism and velocity of the Hainan Plume's retreat, and how the Hainan Plume triggered melting, are still unclear. Further work to perfect this model is needed in the future.

6. Conclusions

Post-rift magmatism in the Baiyun Sag is addressed in this study based on the integration of large 3D/2D seismic volumes tied to borehole data. The main conclusions of this work are as follows:

1. Magmatism is mainly located along the southern shoulder of the Baiyun Sag, where it can be subdivided into three distinct zones. MZ1 is characterized by magma intrusions, interconnected sills and dikes that reveal main magma migration pathways. MZ2 and MZ3 are dominated by the extrusion of magma, with relatively small normal faults comprising the main magma-migration pathways;
2. Early Miocene magmatism occurred in a limited time period (~19.0-17.5 Ma). It was slightly younger when moving from MZ1 to MZ3 due to the increasing migration distances travelled by magma, i.e., from their deep-seated chambers to the loci of magma extrusion and underlying intrusions;
3. The extensive and voluminous early Miocene magmatism documented here probably originated from local mantle upwelling caused by the retreat of the Hainan Plume. This accompanied the readjustment of mantle material due to a jump in the location of the

spreading ridge from the East Sub-basin to the Southwest Sub-basin.

This study addresses the characteristics of post-rift magmatism in the highly stretched Baiyun Sag. More importantly, it provides an answer to the origin of post-rift magmatism in the northern SCS, confirming the Hainan Plume as responsible for the focused magmatism observed in the study area.

Acknowledgements

This work was supported by the National Key R&D Program of China (No. 2018YFC0310000), the National Scientific Foundation of China (Nos. 41676051, 41730532), and the Fundamental Research Funds for the Central Universities-the China University of Geosciences (Wuhan) (No. CUG2106207). The China National Offshore Oil Company (CNOOC) is thanked for permission to release the data. The data that support the findings of this study are available from the CNOOC (http://www.cnooc.com.cn/en/). Restrictions apply to the availability of these data, which were used under license for this study. We are grateful to the Editor-in-Chief M. Santosh and the Guest Editor Sanzhong Li for handling our paper. Dr. Yakufu Niyazi and an anonymous reviewer are thanked for their constructive and thoughtful comments, which significantly improved the quality of this manuscript.

References

Alves, T.M., Omosanya, K., Gowling, P., 2015. Volume rendering of enigmatic high-amplitude anomalies in southeast Brazil: A workflow to distinguish lithologic features from fluid accumulations. Interpretation 3, A1-A14. https://doi.org/10.1190/INT-2014-0106.1.

Berndt, C., Skogly, O.P., Planke, S., Eldholm, O., Mjelde, R., 2000. High-velocity breakup-related sills in the Vøring Basin, off Norway. J. Geophys. Res.-Solid Earth 105, B12. https://doi.org/ 10.1029/2000JB900217.

Briais, A., Patriat, P., Tapponnier, P., 1993. Updated interpretation of magnetic anomalies and seafloor spreading stages in the South China Sea: Implications for the Tertiary tectonics of Southeast Asia. J. Geophys. Res. 98, 6299-6328. https://doi.org/10.1029/92JB02280.

Brown, A. R., 2004, Interpretation of three-dimensional seismic data: AAPG Memoir 42, 6thed. SEG Investigations in Geophysics.

Chen, L., 2014. Stretching factor estimation for the long-duration and multi-stage continental extensional tectonics: Application to the Baiyun Sag in the northern margin of the South China Sea. Tectonophysics 611, 167-180. http://dx.doi.org/10.1016/j.tecto.2013.11.026.

Clift, P., Lin, J., Barckhausen, U., 2002. Evidence of low flexural rigidity and low viscosity lower continental crust during continental break-up in the South China Sea. Mar. Pet. Geol. 19, 951-970. http://dx.doi.org/10.1016/S0264-8172(02)00108-3.

Clift, P.D., Lin, J., and ODP Leg 184 Scientific Party, 2001. Patterns of extension and magmatism along the continent-ocean boundary, South China margin. Geo. Soc. London Special Pub. 187, 489-510. https://doi.org/10.1144/GSL.SP.2001.187.01.24.

Deng, P., Mei, L.F., Liu, J., Zheng, J.Y., Liu, M.H., Cheng, Z.J., Guo, F.T., 2018. Episodic normal faulting and magmatism during the syn-spreading stage of the Baiyun sag in Pearl River Mouth Basin: response to the multi-phase seafloor spreading of the South China Sea. Mar. Geophys. Res. 40, 35-50. https://doi.org/10.1007/s11001-018-9352-9.

Ding, W., Franke, D., Li, J., Steuer, S., 2013. Seismic stratigraphy and tectonic structure from a composite multi-channel seismic profile across the entire Dangerous Grounds, South China Sea. Tectonophysics 582, 162-176. https://doi.org/10.1016/j.tecto.2012.09.026.

Ding, W., Sun, Z., Dadd, K., Fang, Y., Li, J., 2018. Structures within the oceanic crust of the central South China Sea basin and their implications for oceanic accretionary processes. Earth Planet. Sci. Lett. 488, 115-125. https://doi.org/10.1016/j.epsl.2018.02.011.

Fan, C.Y., Xia, S.H., Zhao, F., Sun, J.L., Cao, J.H., Xu, H.L., Wan, K.Y., 2017. New insights into the magmatism in the northern margin of the South China Sea: Spatial features and volume of intraplate seamounts. Geochem. Geophys. Geosyst. 18, 2216-2239. https://doi.org/10.1002/2016GC006792.

Fang, P.G., Ding, W.W., Zhao, Y.H., Lin, X.B., Zhao, Z.X.,

2022. Detachment-controlled subsidence pattern at hyper-extended passive margin: Insights from backstripping modelling of the Baiyun Rift, northern South China Sea. Gondwana Res. in press. https://doi.org/10.1016/j.gr.2021.12.012.

Franke, D., 2013. Rifting, lithosphere breakup and volcanism: comparison of magma-poor and volcanic rifted margins. Mar. Pet. Geol. 43, 63-87. https://doi.org/10.1016/j.marpetgeo.2012.11.003.

Franke, D., Savva,D., Pubellier, M., Steuer, S., Mouly, B., Auxietre, J., Meresse, F., Chamot-Rooke, N., 2014. The final rifting evolution in the South China Sea. Mar. Pet. Geol. 58, 704-720. https://doi.org/10.1016/j.marpetgeo.2013.11.020.

Gong, Z.S., Li, S.T., 1997. Continental Margin Basin Analysis and Hydrocarbon Accumulation of the Northern South China Sea. Science Press, pp. 193–256 (in Chinese with English abstract).

He, E.Y., 2017. The deep crustal structure of the extinct spreading ridge of the East Sub-basin in the South China Sea. PhD Dissertation, pp 118.

Huang, C., Zhou, D., Sun, Z., Chen, C., Hao, H., 2005. Deep crustal structure of Baiyun Sag, northern South China Sea revealed from deep seismic reflection profile. Sci. Bull. 50, 1131-1138. https://doi.org/10.1360/04wd0207.

Huang, X.L., Xu, Y.G., Yang, F., 2020. Basalts in the South China Sea: Mid-ocean ridges and seamounts. Science & Technology Review, 38, 46-51 (in Chinese with English Abstract).

Hui, G.G., Li, S.Z., Li, X.Y., Guo, L.L., Suo, Y.H., Somerville, I.D., Zhao, S.J., Hu, M.Y., Lan, H.Y., Zhang, J., 2016. Temporal and spatial distribution of Cenozoic igneous rocks in the South China Sea and its adjacent regions: implications for tectono-magmatic evolution. Geol. J. 51, 429-447. https://doi.org/10.1002/gj.2801.

Larsen, H.C., Mohn, G., Nirrengarten, M., Sun, Z., Stock, J., Jian, Z., Klaus, A., AlvarezZarikian, C.A., Boaga, J., Bowden, S.A., Briais, A., Chen, Y., Cukur, D., Dadd, K., Ding, W., Dorais, M., Ferr´e, E.C., Ferreira, F., Furusawa, A., Gewecke, A., Hinojosa, J., Hofig, ¨ T.W., Hsiung, K.H., Huang, B., Huang, E., Huang, X.L., Jiang, S., Jin, H., Johnson, B.G., Kurzawski, R.M., Lei, C., Li, B., Li, L., Li, Y., Lin, J., Liu, C., Liu, Z., Luna, A.J., Lupi, C., McCarthy, A., Ningthoujam, L., Osono, N., Peate, D.W., Persaud, P., Qiu, N., Robinson, C., Satolli, S., Sauermilch, I., Schindlbeck, J.C., Skinner, S., Straub, S., Su, X., Su, C., Tian, L., van der Zwan, F.M., Wan, S., Wu, H., Xiang, R., Yadav, R., Yi, L., Yu, P.S., Zhang, C., Zhang, J., Zhang, Y., Zhao, N., Zhong, G., Zhong, L., 2018. Rapid transition from continental breakup to igneous oceanic crust in the South China Sea. Nat. Geosci. 11, 782-789. https://doi.org/10.1038/s41561-018-0198-1.

Lei, C., Ren, J.Y., Pang, X., Chao, P., Han, X.Y., 2018. Continental rifting and sediment infill in the distal part of the northern South China Sea in the Western Pacific region: Challenge on the present-day models for the passive margins. Mar. Pet. Geol. 93, 166-181. https://doi.org/10.1016/j.marpetgeo.2018.02.020.

Lester, R., Van Avendonk, H.J.A., McIntosh, K., Lavier, L., Liu, C.S., Wang, T.K., Wu, F., 2014. Rifting and magmatism in the northeastern South China Sea from wide-angle tomography and seismic reflection imaging. J. Geophys. Res.-Solid Earth, 119, 2305-2323. https://doi.org/10.1002/2013jb010639.

Li, C.F., Xu, X., Lin, J., Sun, Z., et al., 2014. Ages and magnetic structures of the South China Sea constrained by the deep tow magnetic surveys and IODP Expedition 349. Geochem. Geophys. Geosyst. 15, 4958-4983. https://doi.org/10.1002/2014GC005567.

Li, P., Rao, C., 1994. Tectonic characteristics and evolution history of the Pearl River Mouth Basin. Tectonophysics, 235, 13-25. https://doi.org/10.1016/0040-1951(94)90014-0.

Li, S.Z., Li, X.Y., Zhou, J., Cao, H.H., Liu, L,J., Liu, Y.M., Sun, G.Z., Suo, Y.H., Li, Y., Yu, S.Y., Jiang, Z.X., 2022. Passive magmatism on Earth and Earth-like planets. Geosyst. Geoenviron. 1, 100008. https://doi.org/10.1016/j.geogeo.2021.10.003.

Li, S.Z., Suo, Y.H., Li, X.Y., Zho, J., Santosh, M., Wang, P.C., Wang, G.Z., Guo, L.L., Yu, S.Y., Lan, H.Y., Dai, L.M., Zhou, Z.Z., Cao, X.Z., Zhu, J.J., Liu, B., Jiang, S.H., Wang, G., Zhang, G.W., 2019. Mesozoic tectono-magmatic response in the East Asian ocean-continent connection zone to subduction of the Paleo-Pacific Plate. Earth-Sci. Rev. 192, 91-137. https://doi.org/10.1016/j.earscirev.2019.03.003.

Lüdmann, T., Wong, H.K., 1999. Neotectonic regime at the passive continental margin of northern South China Sea.

Tectonophysics 311, 113-138. https://doi.org/10.1016/S0040-1951(99)00155-9.

Ma, B.J., Wu, S.G., Betzler, C., Qin, Z.L., Mi, L.J., Gao, W., Bai, H.Q., Wu, F., Dong, D.D., 2018. Geometry, internal architecture, and evolution of buried volcanic mounds in the northern South China Sea. Mar. Pet. Geol. 97, 540-555. https://doi.org/10.1016/j.marpetgeo.2018.07.029.

Magee, C., Hunt-Stewart, E., Jackson, C.A.-L., 2013. Volcano growth mechanism and the role of sub-volcano intrusions: insight from 2D seismic reflection data. Earth Planet. Sci. Lett. 373, 41-53. https://doi.org/10.1016/j.epsl.2013.04.041.

Menzies, M.A., Fan, W., Zhang, M., 1993. Palaeozoic and Cenozoic lithoprobes and the loss of >120 km of Archaean lithosphere, SinoKorean craton, China. Geol. Soc. Spec. Publ. 76, 71-81.

Niyazi, Y., Eruteya, O.E., Warne, M., Ierodiaconou, D., 2021a. Discovery of large-scale buried volcanoes within the Cenozoic succession of the Prawn Platform, offshore Otway Basin, southeastern Australia. Mar. Pet. Geol. 123, 104747. https://doi.org/10.1016/j.marpetgeo.2020.104747.

Niyazi, Y., Warne, M., Ierodiaconou, D., 2021b. Post-rift magmatism and hydrothermal activity in the central offshore Otway Basin and implications for magmatic plumbing systems. Mar. Geol. 438, 106538. https://doi.org/10.1016/j.margeo.2021.106538.

Pang, X., Chen, C.M., Peng, D.J., Zhou, D., Shao, L., He, M., Liu, B.J., 2008. Basic geology of Baiyun deep-water area in the northern South China Sea. China Offshore Oil Gas, 20, 216-222 (in Chinese with English Abstract).

Pang, X., Ren, J.Y., Zheng, J.Y., Liu, J., Peng, Y., Liu, B.J., 2018. Petroleum geology controlled by extensive detachment thinning of continental margin crust: A case study of Baiyun sag in the deep-water area of northern South China Sea. Petroleum Explor. Dev. 45, 29-42.

Peron-Pinvidic, G., Manatschal, G., 2010. From microcontinents to extensional allochthons: witnesses of how continents rift and break apart? Petrol. Geosci. 16, 189-197. https://doi.org/10.1007/978-3-540-87656-4_79.

Qin, G.Q., 1996. Application of micropaleontology to the sequence stratigraphic studies of late Cenozoic in the Zhujiang River Mouth Basin. Mar. Geol. & Quat. Geol. 16, 1-17 (in Chinese with English Abstract).

Qin, G.Q. 2000. Comments on “Discussion on the Upper-Lower Tertiary boundary in Well BY7-1” of the Pearl River Mouth Basin. J. Stratigr. 24, 387-393 (in Chinese with English Abstract).

Reynolds, P., Holford, S., Schofield, N., Ross, A., 2017. Three-dimensional seismic imaging of ancient submarine lava flows: An example from the southern Australian margin: Geochem. Geophys. Geosyst. 18, 3840-3853. https://doi.org/10.1002/2017GC007178.

Reynolds, P., Schofield, N., Brown, R.J., Holford, S.P., 2018. The architecture of submarine monogenetic volcanoes - insights from 3D seismic data. Basin Res. 30, 437-451. https://doi.org/10.1111/bre.12230

Rohrman, M., 2013. Intrusive large igneous provinces below sedimentary basins: An example from the Exmouth Plateau (NW Australia): Intrusive large igneous provinces. J. Geophys. Res. 118, 4477-4487. https://doi.org/10.1002/jgrb.50298.

Ru, K., Pigott, J.D., 1986. Episodic rifting and subsidence in the South China Sea. AAPG Bull. 9, 1136-1155. https://doi.org/10.1306/94886d5d-1704-11d7-8645000102c1865d.

Schofield, N., Holford, S., Millett, J., Brown, D., Jolley, D., Passey, S., Muirhead, D., Grove, C., Magee, C., Murray, J., Hole, M., Jackson, C., Stevenson, C., 2017. Regional Magma Plumbing and emplacement mechanisms of the Faroe-Shetland Sill Complex: implications for magma transport and petroleum systems within sedimentary basins. Basin Res. 29, 41-63. https://doi.org/10.1111/bre.12164.

Sibuet, J.-C., Yeh, Y.-C., Lee, C.-S., 2016. Geodynamics of the South China Sea: Tectonophysics, 692, 98-119. https://doi.org/10.1016/j.tecto.2016.02.022.

Smallwood, J.R., Maresh, J., 2002. The properties, morphology and distribution of igneous sills: modelling, borehole data and 3D seismic from the Faroe-Shetland area. Geo. Soc. London Special Pub. 197, 271-306. https://doi.org/10.1144/GSL.SP.2002.197.01.11.

Song, X., Li, C., Yao, Y., Shi, H., 2017. Magmatism in the evolution of the South China Sea: Geophysical characterization. Mar. Geol. 394, 4-15. https://doi.org/10.1016/j.margeo.2017.07.021.

Sun, Q.L., Alves, T.M., Zhao, M.H., Sibuet, J-C., Calvès, G., Xie, X.N., 2020b. Post-rift magmatism on the

northern South China Sea margin. GSA Bull. 132, 2382-2396. https://doi.org/10.1130/B35471.1.

Sun, Q.L., Jackson, C.A.L., Magee, C., Mitchell, S.J., Xie, X.N., 2019. Extrusion dynamics of deepwater volcanoes revealed by 3-D seismic data. Solid Earth, 10, 1269-1282. https://doi.org/10.5194/se-10-1269-2019.

Sun, Q.L., Jackson, C.A.L., Magee, C., Xie, X.N., 2020c. Deeply buried ancient volcanoes control hydrocarbon migration in the South China Sea. Basin Res. 32, 146-162. https://doi.org/10.1111/bre.12372.

Sun, Q.L., Magee, C., Jackson, C.A.L., Mitchell, S.J., Xie, X.N., 2020a. How do deep-water volcanoes grow? Earth Planet. Sci. Lett. 542, 116320. https://doi.org/10.1016/j.epsl.2020.116320.

Sun, Q.L., Wang, C., Xie, X.N., 2022. Sill swarms and hydrothermal vents in the Qiongdongnan Basin, northern South China Sea. Geosyst. Geoenviron. in press. https://doi.org/10.1016/j.geogeo.2022.100037.

Sun, Q.L., Wu, S.G., Cartwright, J., Wang, S.H., Lu, Y.T., Chen, D.X., Dong, D.D., 2014. Neogene igneous intrusions in the northern South China Sea: evidence from high resolution three dimensional seismic data. Mar. Pet. Geol. 54, 83-95. https://doi.org/10.1016/j.marpetgeo.2014.02.014.

Sun, Z., Lin, J., Qiu, N., Jian, Z.M., Wang, P.X., Pang, X., Zheng, J.Y., Zhu, B.D., 2019b. The role of magmatism in the thinning and breakup of the South China Sea continental margin. Natl. Sci. Rev. 6 (5), 871-876. https://doi.org/10.1093/nsr/nwz116.

Sun, Z., Xu, Z., Sun, L., Pang, X., Yan, C., Li, Y., Zhao, Z., Wang, Z., and Zhang, C. 2014b. The mechanism of post-rift fault activities in the Baiyun Sag, Pearl River Mouth Basin. J. Asian Earth Sci. 89, 76-87. https://doi.org/10.1016/j.jseaes.2014.02.018.

Thomson, K., Hutton, D., 2004. Geometry and growth of sill complexes: insights using 3D seismic from the North Rockall Trough. Bull. Volcanol. 66, 364-375. https://doi.org/10.1007/s00445-003-0320-z.

Trude, J., Cartwright, J., Davies, R.J., and Smallwood, J., 2003. New technique for dating igneous sill. Geology 31, 813-816. https://doi.org/10.1130/G19559.1.

Wang, J.H., Pang, X., Tang, D.Q., Liu, B.J., Xu, D.H., 2013. Transtensional tectonism andits effects on the distribution of sandbodies in the Paleogene Baiyun Sag, Pearl River Mouth Basin, China. Mar. Geophys. Res. 34, 195-207. http://dx.doi.org/10.1007/s11001-013-9200-x.

Wang, K., Lo, Y., Chung, S., Lo, C., Hsu, S., Yang, H., Shinjo, R., 2012. Age and geochemical features of dredged basalts from offshore SW Taiwan: the coincidence of Intra-Plate magmatism with the spreading South China Sea. Terr. Atmos. Ocean. Sci. 23, 657-669. https://doi.org/10.3319/TAO.2012.07.06.01(TT).

White, R., McKenzie, D., 1989. Magmatism at the rift zones: the generation of volcanic continental margins and flood basalts. J. Geophys. Res. 94, 7685-7729. https://doi.org/10.1029/JB094iB06p07685.

Xia, S.H., Zhao, F., Zhao, D.P., Fan, C.Y., Wu, S.G., Mi, L.J., Sun, J.L., Cao, J.H., Wan, K.Y., 2018. Crustal plumbing system of post-rift magmatism in the northern margin of South China Sea: New insights from integrated seismology. Tectonophysics 744, 227-238. https://doi.org/10.1016/j.tecto.2018.07.002.

Xie, H., Zhou, D., Li, Y.P., Pang, X., Li, P.X., Chen, G.H., Li, F.C., Cao, J.H., 2014. Cenozoic tectonic subsidence in deepwater sags in the Pearl River Mouth Basin, northern South China Sea. Tectonophysics 615-616, 182-198. https://doi.org/10.1016/j.tecto.2014.01.010.

Xu, Y. G., Sun, M., Yan, W., Liu, Y., Huang, X. L., Chen, X. M. 2002. Xenolith evidence for polybaric melting and stratification of the upper mantle beneath South China. J. Asian Earth Sci., 20(8): 937–954. https://doi.org/10.1016/S1367-9120(01)00087-6.

Xu, Y.G., Wei, J., Qiu, H., Zhang, H., Huang, X., 2012. Opening and evolution of the South China Sea constrained by studies on volcanic rocks: Preliminary results and a research design. Chinese Sci. Bull., 57(24): 3150-3164, https://doi.org/10.1007/s11434-011-4921-1.

Yan, P., Deng, H., Liu, H.L., Zhang, Z., Jiang, Y., 2006. The temporal and spatial distribution of volcanism in the South China Sea region. J. Asian Earth Sci. 27, 647-659. https://doi.org/10.1016/j.jseaes.2005.06.005.

Yan, Q., Shi, X., Castillo, P.R., 2014. The late Mesozoic-Cenozoic tectonic evolution of the South China Sea: A petrologic perspective. J. Asian Earth Sci. 27, 647-659. https://doi.org/10.1016/j.jseaes.2005.06.005

Yan, Q., Shi, X., Metcalfe, I., Liu, S., Xu, T., Kornkanitnan, N., Sirichaiseth, T., Yuan, L., Zhang, Y., Zhang, H., 2018. Hainan mantle plume produced late Cenozoic basaltic rocks in Thailand, Southeast Asia. Sci Rep 8, 2640.

https://doi.org/10.1038/s41598-018-20712-7

Yang, L., Ren, J., McIntosh, K., Pang, X., Lei, C., Zhao, Y., 2018. The structure and evolution of deepwater basins in the distal margin of the northern South China Sea and their implications for the formation of the continental margin. Mar. Pet. Geol. 92, 234-254. https://doi.org/10.1016/j.marpetgeo.2018.02.032.

Yu, M.M., Yan, Y., Huang, C.Y., Zhang, X.C., Tian, Z.X., Chen, W.H., Santosh, M., 2018. Opening of the South China Sea and upwelling of the Hainan plume. Geophys. Res. Lett. 45, 2600-2609. https://doi.org/10.1002/2017GL076872

Zhang, C., Sun, Z., Manatschal, G., Pang, X., Qiu, N., Su, M., Zheng, J., Li, H., Gu, Y., Zhang, J., Zhao, Y., 2021. Syn-rift magmatic characteristics and evolution at a sediment-rich margin: Insights from high-resolution seismic data from the South China Sea. Gondwana Res. 91, 81-96. https://doi.org/10.1016/j.gr.2020.11.012.

Zhang, G.L., Chen, L. H., Jackson, M.G., Hofmann, A.W., 2017. Evolution of carbonated melt to alkali basalt in the South China Sea. Nat. Geosci. 10, 229-235. https://doi.org/10.1038/NGEO2877.

Zhao, F., Alves, T.M., Wu, S.G., Li, W., Huuse, M., Mi, L.J., Sun, Q.L., Ma, B.J., 2016. Prolonged post-rift magmatism on highly extended crust of divergent continental margins (Baiyun Sag, South China Sea). Earth Planet. Sci. Lett. 445, 79-91. https://doi.org/10.1016/j.epsl.2016.04.001.

Zhao, F., Wu, S.G., Sun, Q.L., Huuse, M., Li, W., Wang, Z.J., 2014. Submarine volcanic mounds in the Pearl River Mouth Basin, northern South China Sea. Mar. Geol. 355, 162-172. https://doi.org/10.1016./j.margeo.2014.05.018.

Zhao, M., He, E., Sibuet, J.-C., Sun, L., Qiu, X., Tan, P., Wang, J., 2018b. Postseafloor spreading volcanism in the central east South China Sea and its formation through an extremely thin oceanic crust. Geochem. Geophys. Geosyst. 19, 621-641. https://doi.org/10.1002/2017GC007034.

Zhao, Y.H., Ren, J.Y., Pang, X., Yang, L.L., Zheng, J.Y., 2018a. Structural style, formation of low angle normal fault and its controls on the evolution of Baiyun Rift, northern margin of the South China Sea. Mar. Pet. Geol. 89, 687-700. https://doi.org/10.1016/j.marpetgeo.2017.11.001.

Zhou, Z.C., Mei, L.F., Liu, J., Zheng, J.Y., Chen, L., Hao, S.H., 2018. Continentward-dipping detachment fault system and asymmetric rift structure of the Baiyun Sag, northern South China Sea. Tectonophysics 726, 121-136. https://doi.org/10.1016/j.tecto.2018.02.002.

Zou, H., Li, P., Rao, C., 1995. Geochemistry of Cenozoic volcanic rocks in Zhu Jiangkou basin and its geodynamic significance. Geochimica, 24, 33-45 (in Chinese with English abstract).

Figures

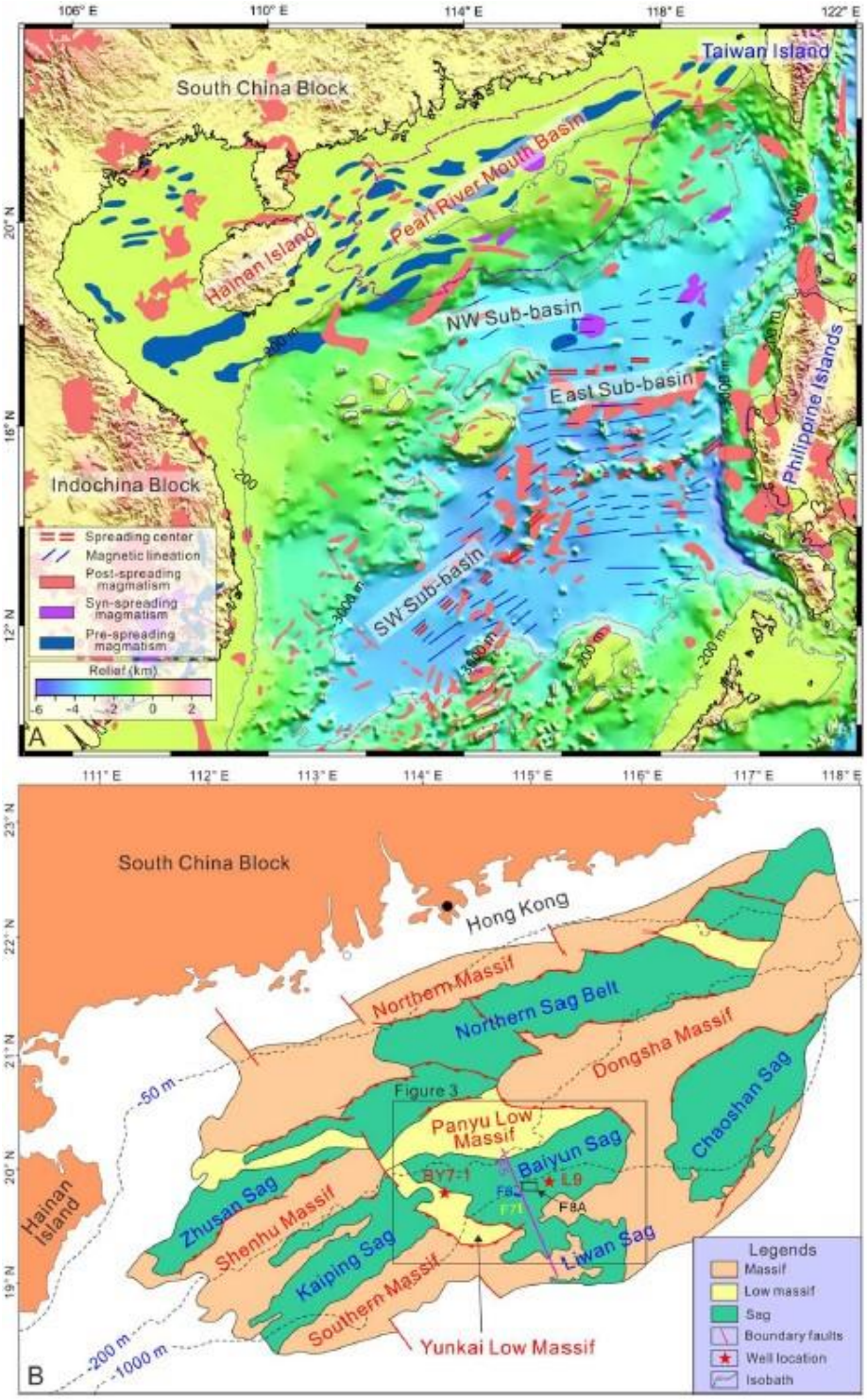

Figure 1. A: Geological setting of the northern South China Sea showing the Northwest (NW), East and Southwest (SW) sub-basins. The base map in this figure was re-drawn from He (2017). The locations of the spreading centre and magnetic lineations are from Briais et al. (1993) and Li et al. (2014). Pre-, syn- and post-spreading magmatism is modified from Hui et al. (2016); B: Geological subdivision of the Pearl River Mouth Basin. Wells BY7-1 and L9 are marked by red stars. The listric boundary faults (detachment faults) are modified from Pang et al. (2008) and Sun et al. (2014). This study is focused on the Baiyun Sag. F4-F7 indicate Figures 4 to 7.

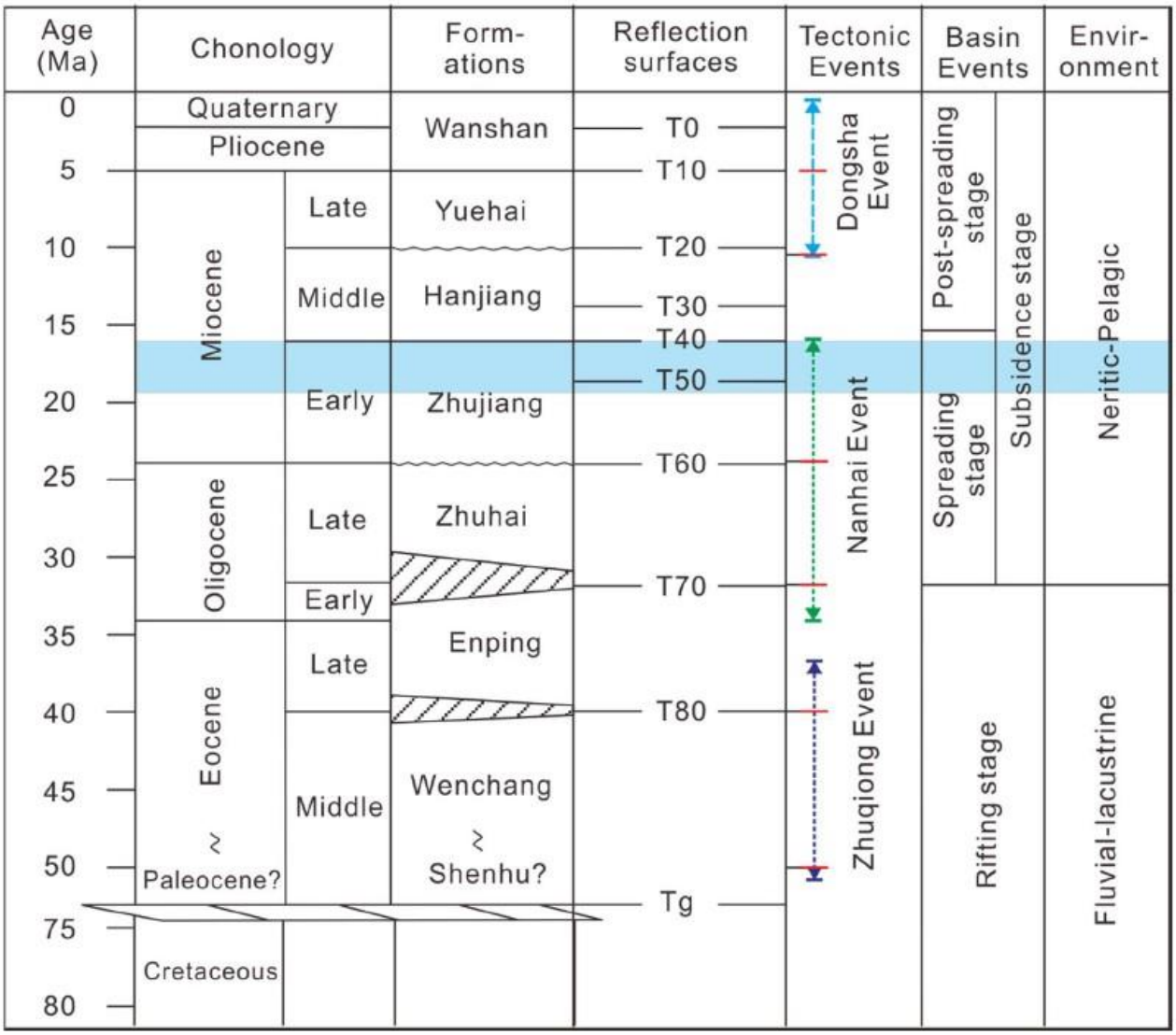

Figure 2: Stratigraphy of the Pearl River Mouth Basin highlighting major tectonic episodes that affected the study area as recognized in Pang et al. (2008) and Sun et al. (2020b). The red lines in 'Tectonic Events' represent the latter tectonic episodes. Magmatism mostly occurred during the early Miocene (blue rectangle).

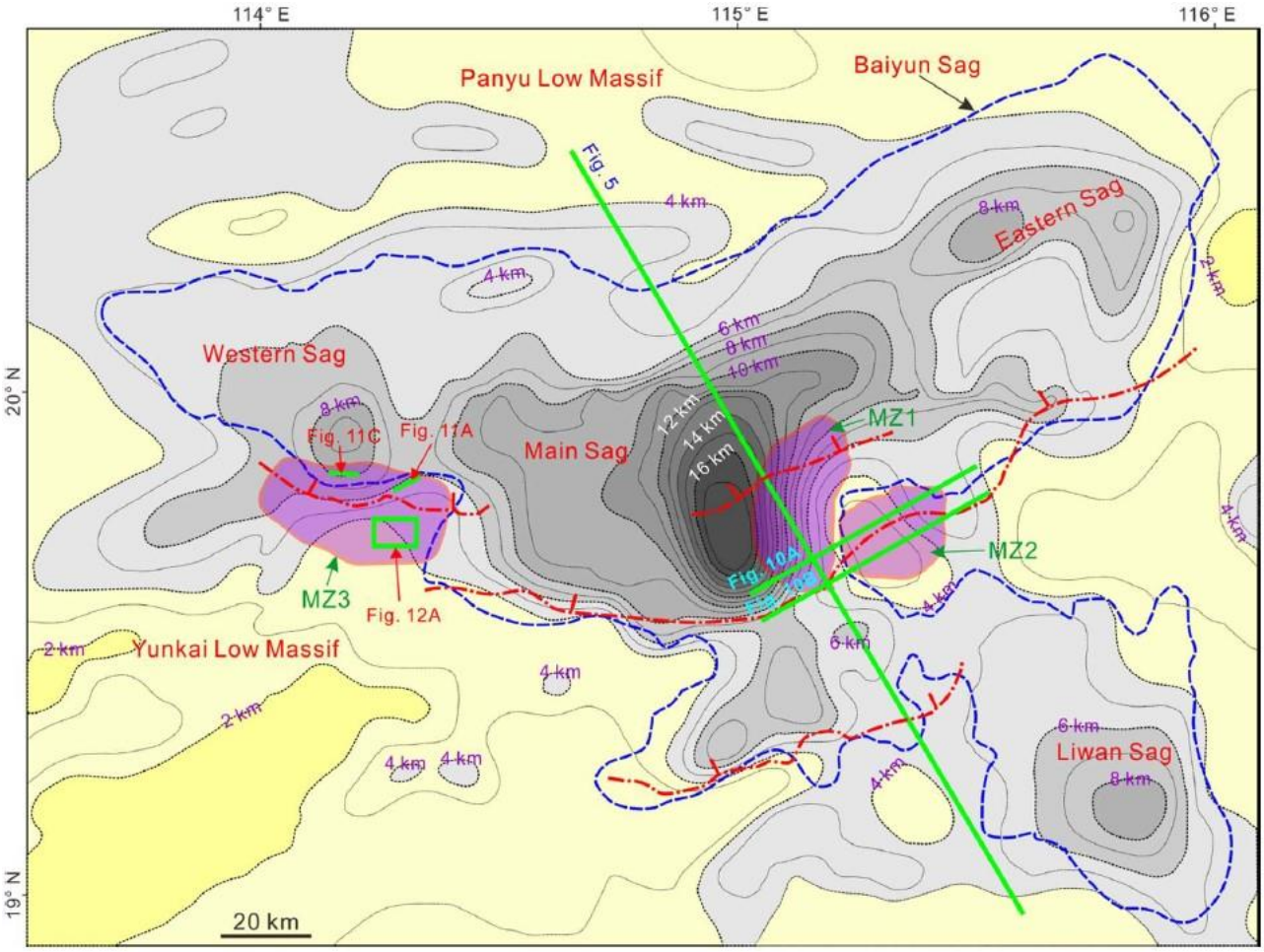

Figure 3: Distribution of magmatic zones in and around the Baiyun Sag (blue dashed lines) superimposed on the burial depth map for the Cenozoic basement (horizon Tg). The isobaths of the burial depth map of the Cenozoic basement are from Yang et al. (2015). The three magmatic zones MZ1, MZ2 and MZ3 (see purple polygons) reflect the locations where magmatic edifices (sills, lava flows and volcanoes) are identified. MZ1 is located on the southern shoulder of the Baiyun Sag, near the deepest part of the Baiyun Sag. MZ2 is located to the southeast of MZ2 over a local high. MZ3 is located on the southern shoulder of the Baiyun Sag. Listric boundary faults (major boundary faults; Wang et al., 2013; Zhou et al., 2018) shown by the red dashed lines are located below and around the magmatic edifices. The location of Figures 5 and 10 are marked.

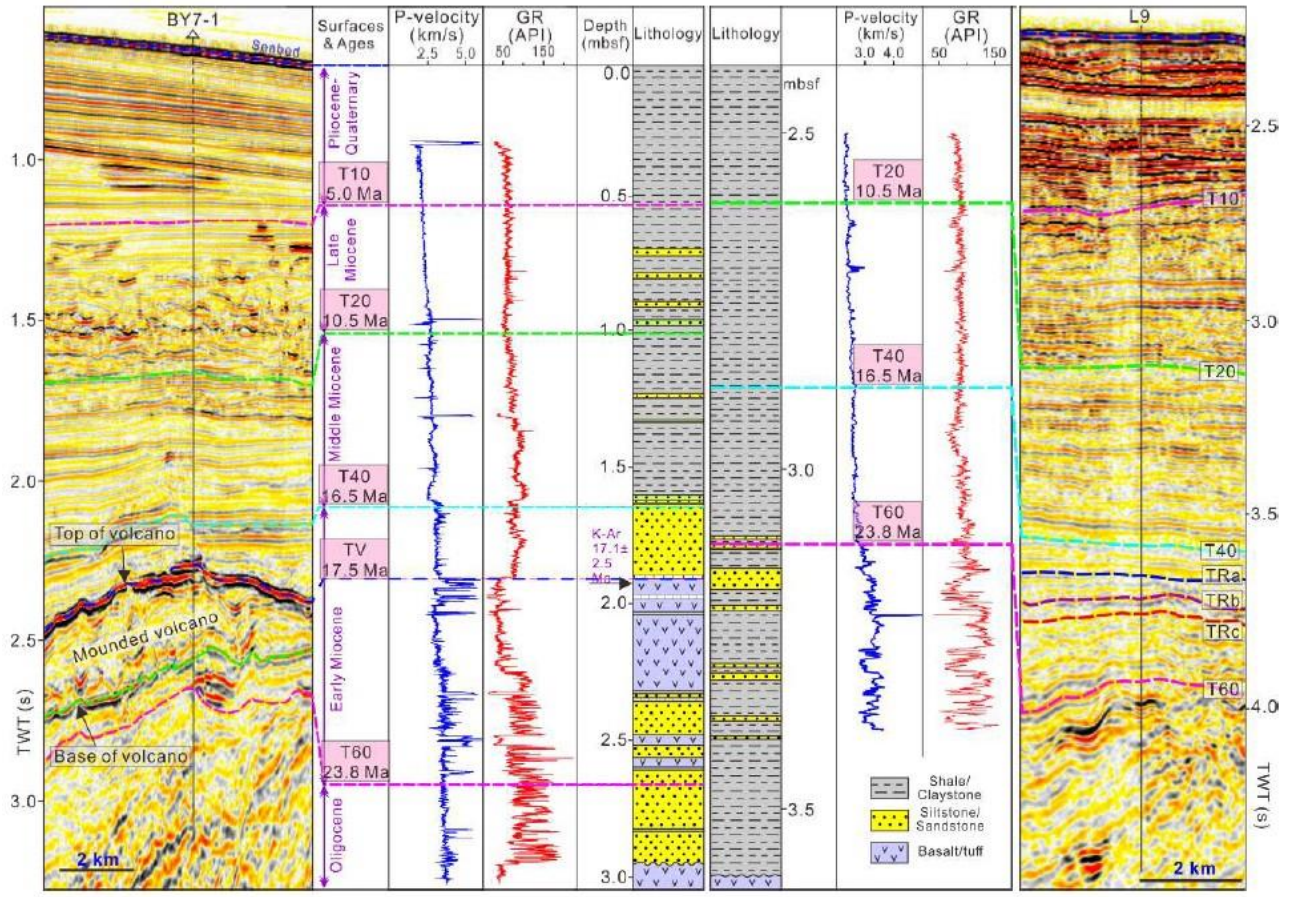

Figure 4: Sequence stratigraphy and lithology of wells BY7-1 and L9. Data for well BY7-1 are modified from Sun et al. (2020c). Principal seismic-stratigraphic horizons (TRa = ~17.5 Ma, TRb = ~18.5 Ma, TRc = ~19.0 Ma) are marked in the figure. The K-Ar age from the top of a mounded volcano is taken from from Qin (1996). GR = Gamma ray; TWT = two-way travel time.

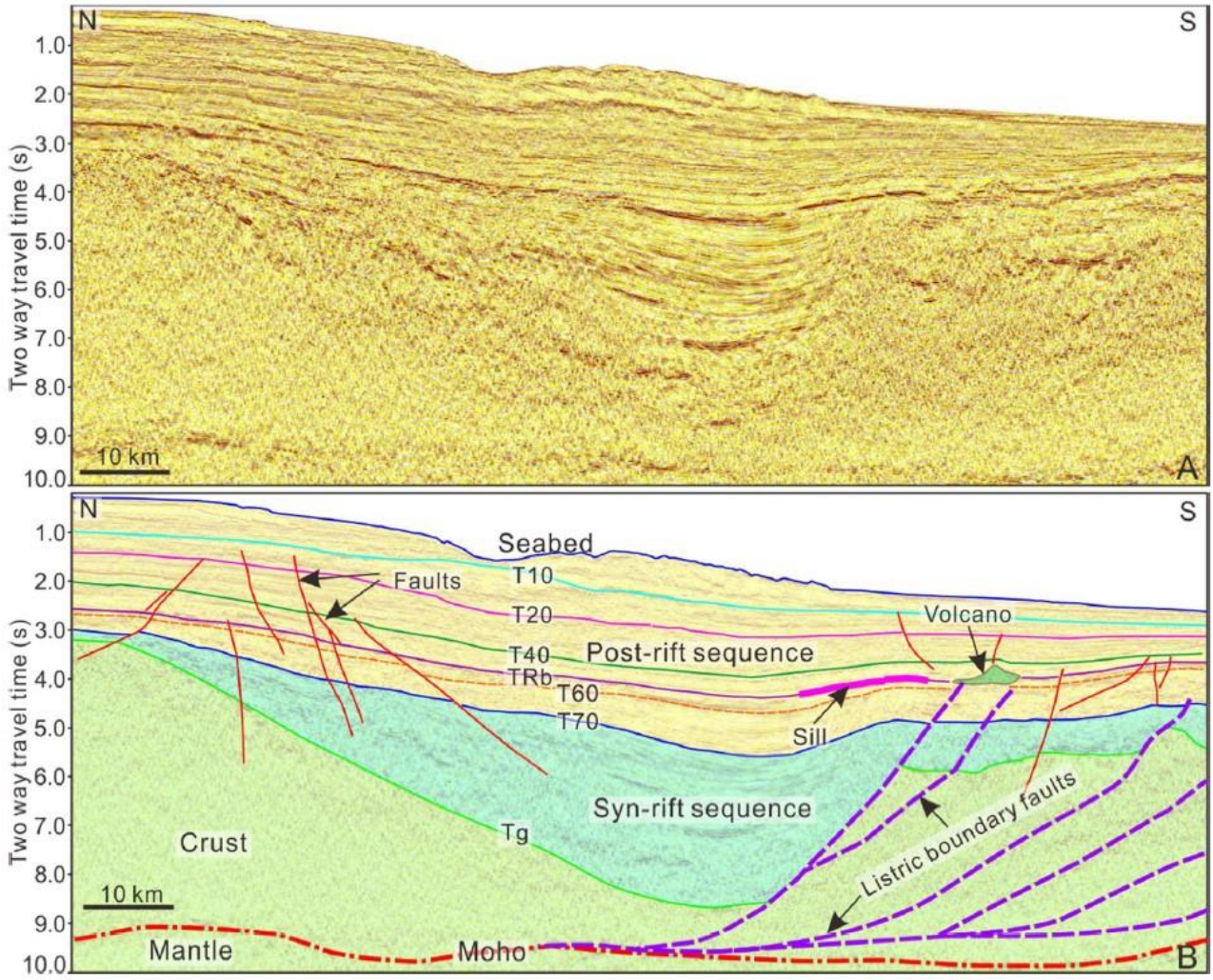

Figure 5: A and B: 2D seismic profile and its interpretation crossing the main depocentre in the Baiyun Sag. See location of the profile in Figures 1 and 3. Syn- and post-rift sequences are separated by horizon T70 (~33 Ma). Low-angle landward listric boundary faults delimit the the southern shoulder of the Baiyun Sag. Magmatic edifices, sills and volcanoes are located above these listric boundary faults, within post-rift strata bounded by horizons T60 and T40. The Moho is shown on the seismic profile as a series of discontinuous high-amplitude reflections at a depth between 9s and 10s two-way time.

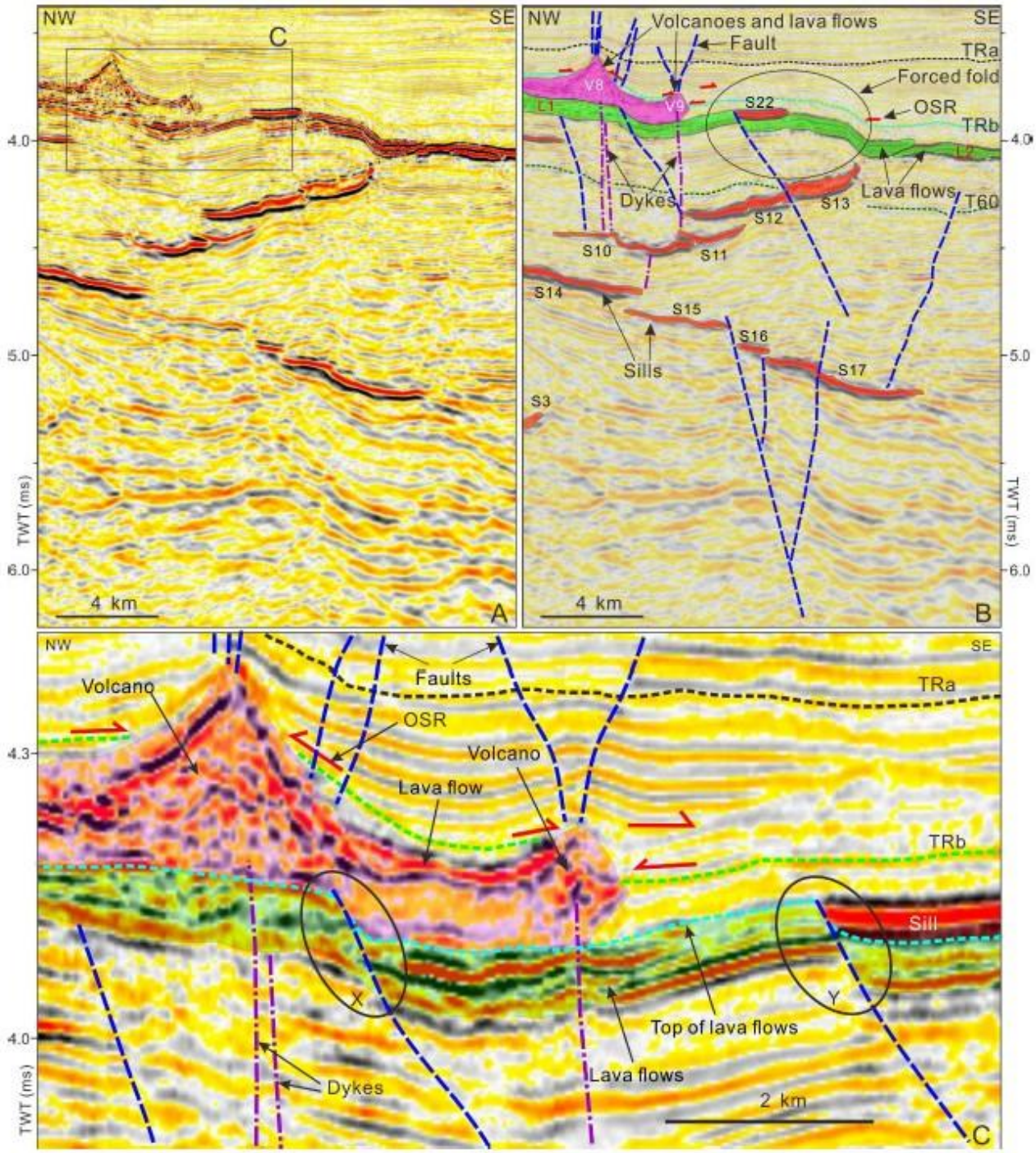

Figure 6: A and B: 3D seismic profile and its interpretation showing magmatic features in MZ1. Sills step upward with the lower sills (in red) feeding the upper ones. Lava flows (in green) with constant thickness and volcanoes (mounded edifices in pink) are linked to the underlying sills via igneous dikes. Forced folds (black ellipse) occur above the sills. Onlapping seismic reflections (OSRs) are observed over horizon TRb near forced folds and volcanoes. Faults and folded strata are also observed above the volcanoes. C: Zoomed-in inset showing lava flows offset by normal faults (see ellipses X and Y). Note that the thickness of the lava flows is similar on the footwalls and adjacent hanging-walls.

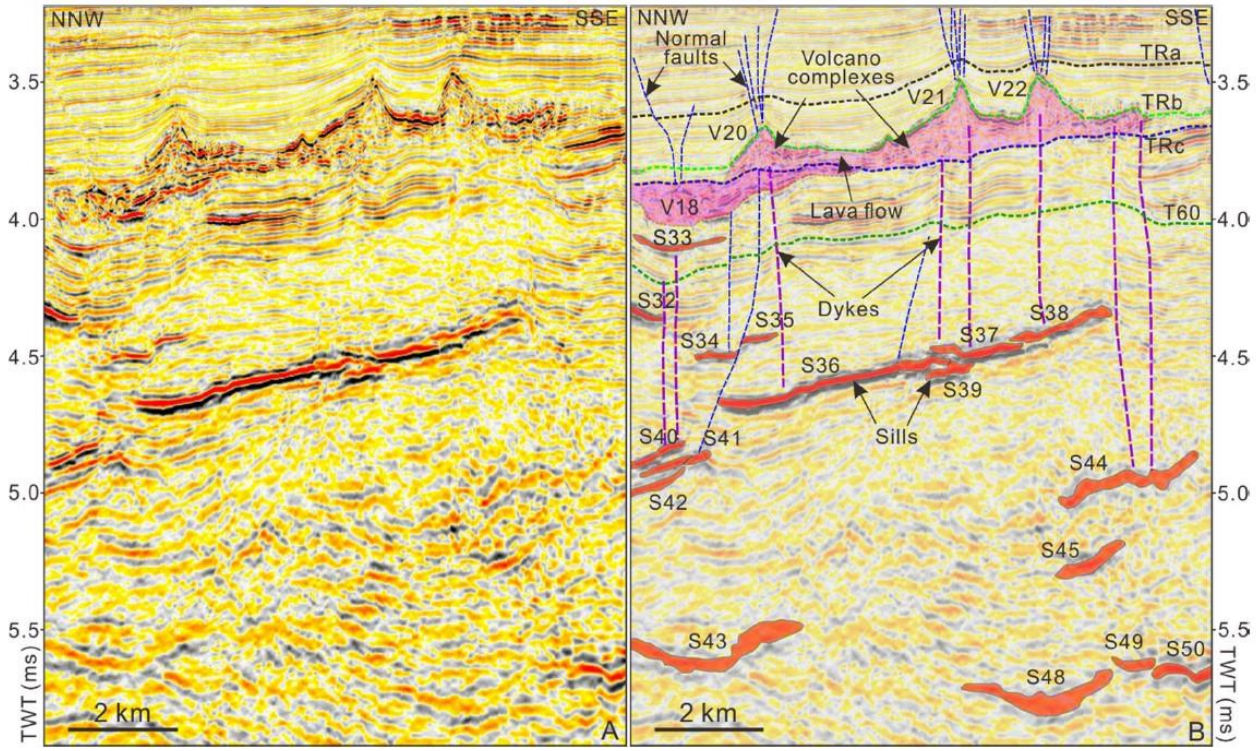

Figure 7: A and B: 3D seismic profile and its interpretation showing magmatic features in MZ1. Saucer and oblique sills with high-amplitude seismic reflections occur deep on the seismic profile. Volcanic complexes with mounded shapes (V20-V22) and chaotic internal seismic reflections are directly onlapped by horizon TRb. V18 is draped by horizon TRc. Dikes are characterized by narrow, vertical wipe-out zones. Faults that offset the strata link the volcanic complexes to deep-seated sills.

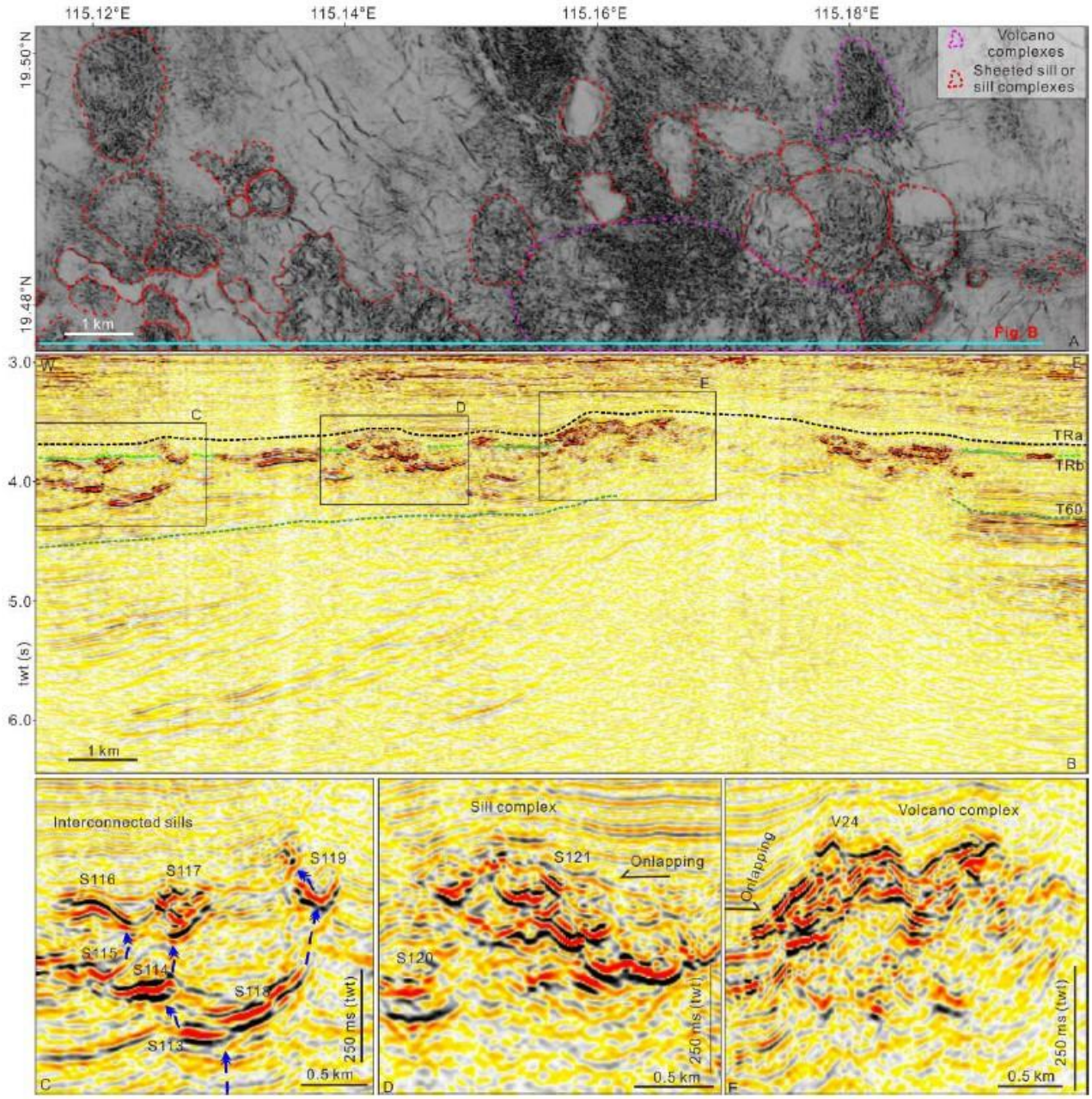

Figure 8: Seismic character of magmatic complexes in MZ1. A: Coherence slice at T=3800 ms (twt) highlighting the presence of sheeted sills (low coherence), sill complexes (medium-high coherence) and volcanic complexes (high coherence). Note that the outlines of sills are based on the interpretation of seismic profiles and coherence slices. B: Seismic profile showing igneous edifices between horizons TRa and T60. Horizon TRb directly onlaps mounded, intrusive and extrusive edifices. C: Interconnected sills. The saucer-shaped sills at shallow depths are fed by the deeper sills. The blue dashed arrows indicate principal magma pathways. D: Sill complex. Saucer sills intruded into the shallow strata and deformed it, generating forced folds. Onlapping seismic reflections are observed on the flank of the forced folds. E: Volcanic complex composed of high-amplitude, convex-upward seismic reflections. Sills intrude the rocks below the volcano edifice. Onlapping seismic reflections are observed on the flanks of the volcano edifice.

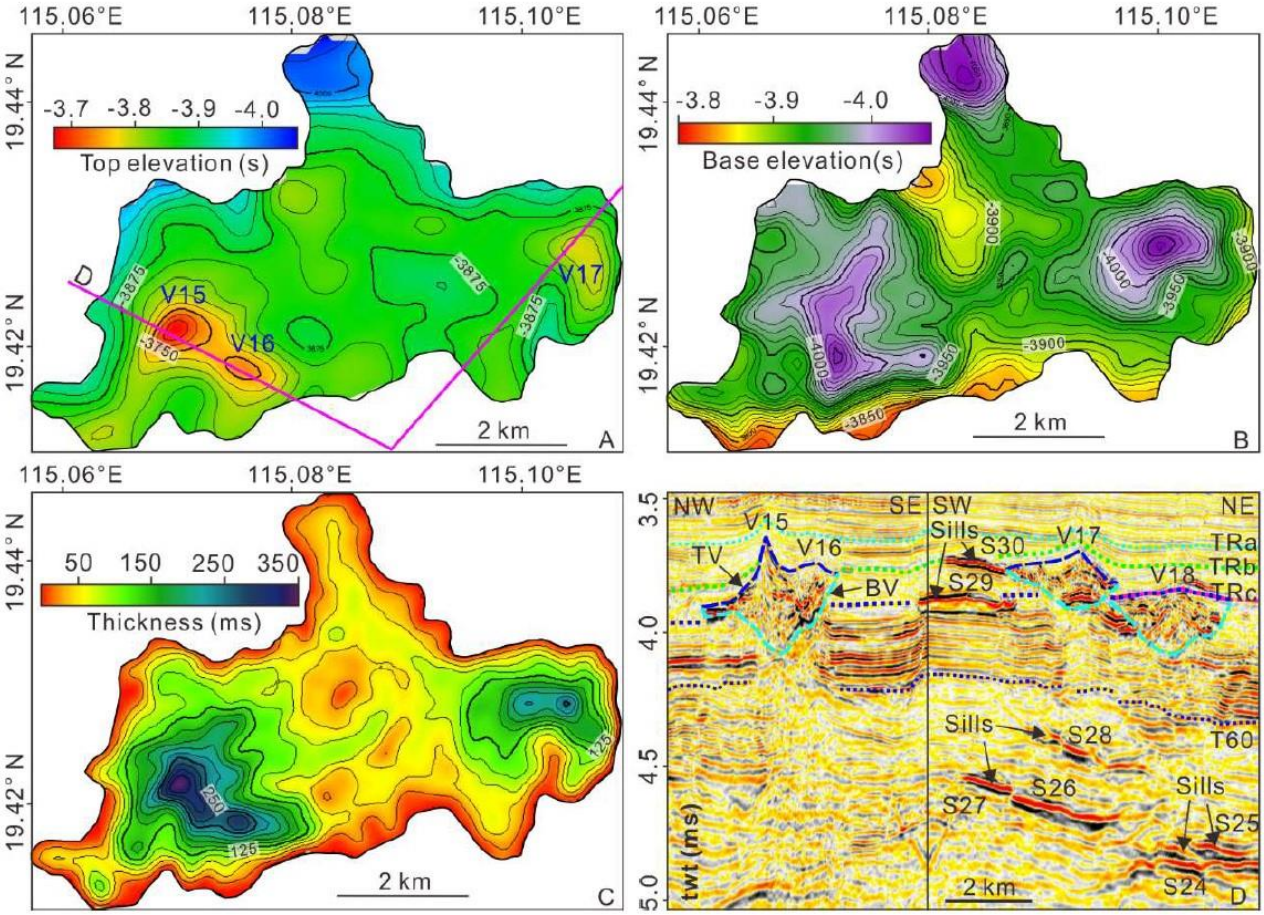

Figure 9: A: Morphology of the top surface of volcanoes V15, V16 and V17 in MZ1. B: Morphology of the basal surface of volcanoes V15, V16 and V17. C: Thickness of volcanoes V15, V16 and V17. D: Seismic profile showing the top (blue dashed lines) and base (cyan dashed lines) of volcanoes V15, V16, V17 and V18. Note that V18 is a slightly older than volcanoes V15-V17, though not shown in Figs. A-C. Horizons TRa, TRb, TRc, T60 and sills and high-amplitude, positive seismic reflections and cross-cutting the stratigraphic succession are marked in the figure.

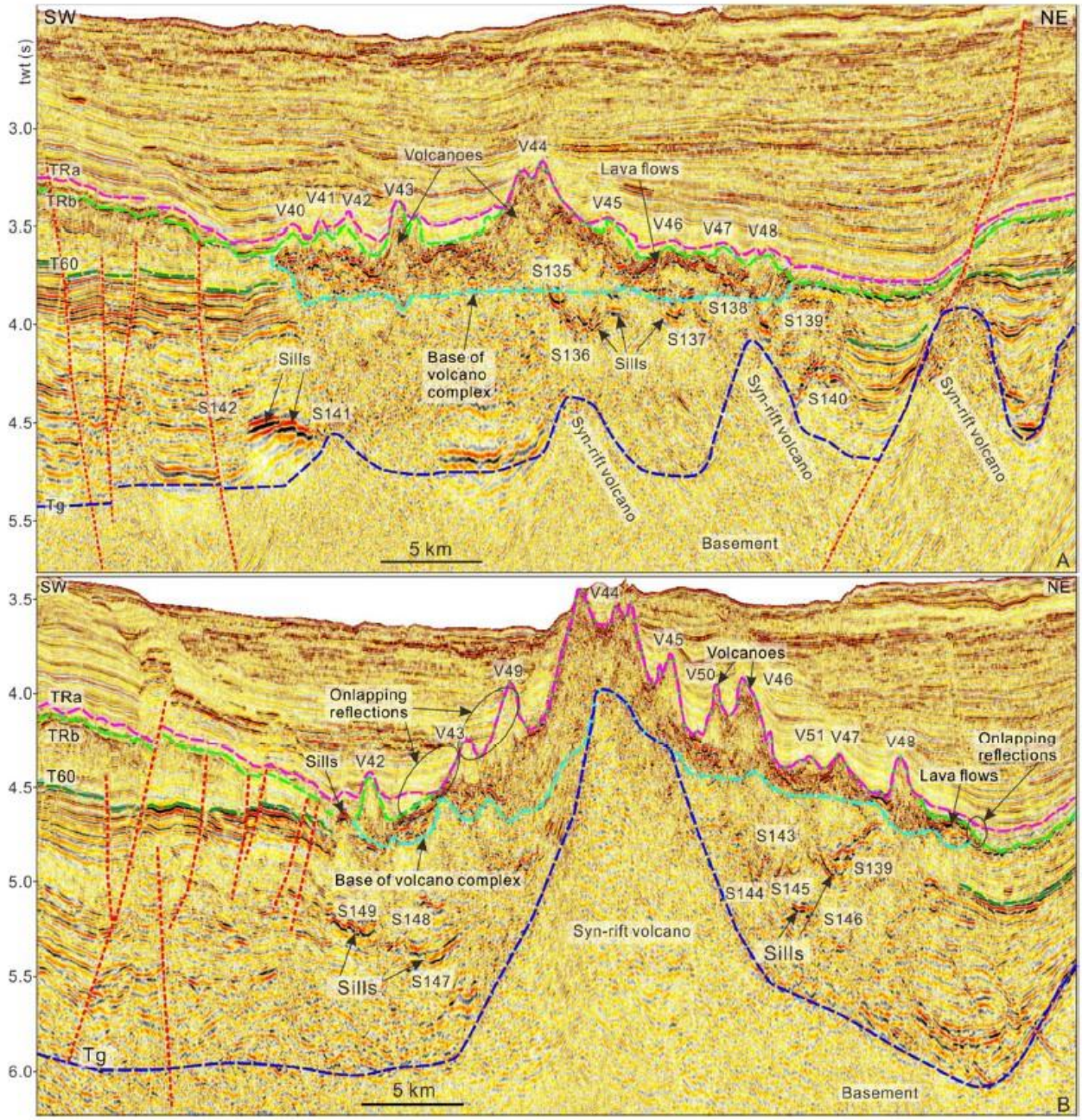

Figure 10: A and B: 2D seismic profiles and their interpretations highlighting the character of magmatic features in MZ2. Volcano edifices are mounded edifices with chaotic internal seismic reflections. Lava flows comprise stacked, high-amplitude seismic reflections and are located around the volcano edifices. Sills are often saucer-shaped and located below the volcanic complexes. TRb directly onlap the volcanic complexes. Syn-rift volcanoes sourced from the basement are also identified and underlie the lower Miocene volcanic complexes. See location of the seismic profile in Figure 3.

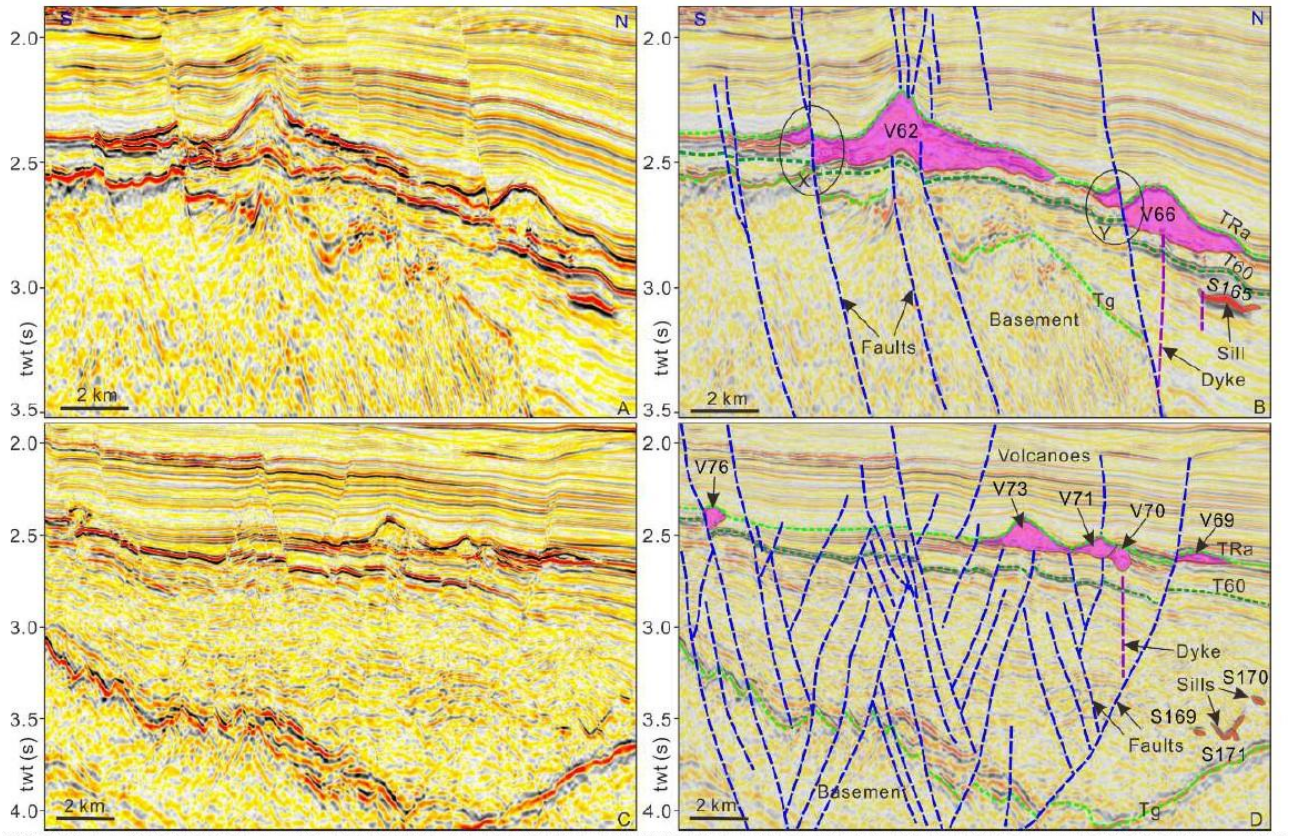

Figure 11: Seismic profiles and their interpretations revealing the character of magmatic features in MZ3. Note that normal faults occur below the volcanoes. Erupted lava on footwalls are thicker than in the adjacent hanging-wall blocks (see X and Y in Figure 11B). Volcanoes in MZ3 are topped by horizon TRa.

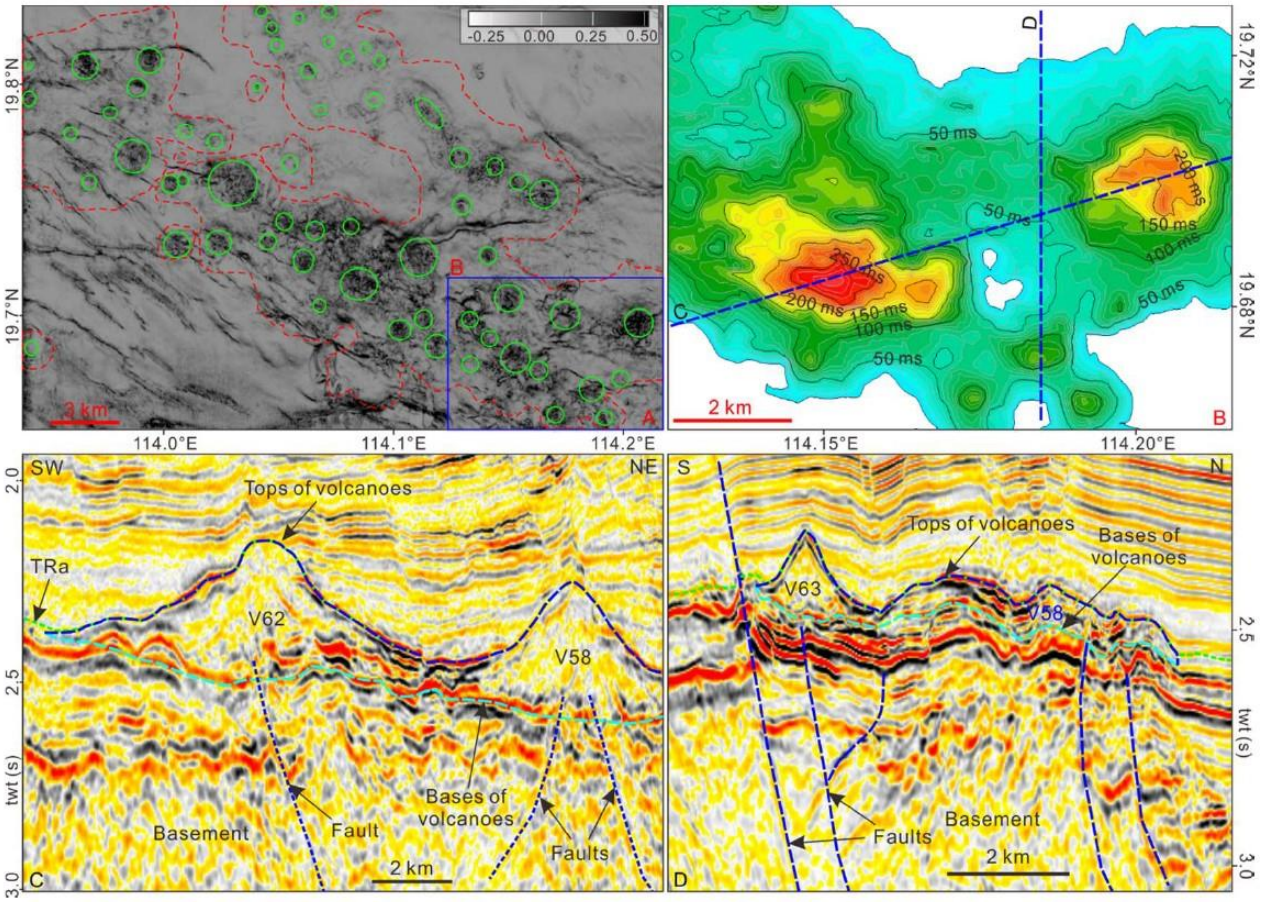

Figure 12: A: Variance slice from a depth 50 ms below horizon TRa highlighting the relative distribution of volcanoes (red dashed line). Volcano tops are marked by green circles. The location of Fig. B is shown in the figure; B: Thickness of volcanoes in the study area; C and D: seismic profiles intersecting volcanoes V58, V62 and V63. Faults are observed below the volcano edifices. The tops (blue dashed lines) and bases of volcanoes (cyan dashed lines) are shown in the figure.

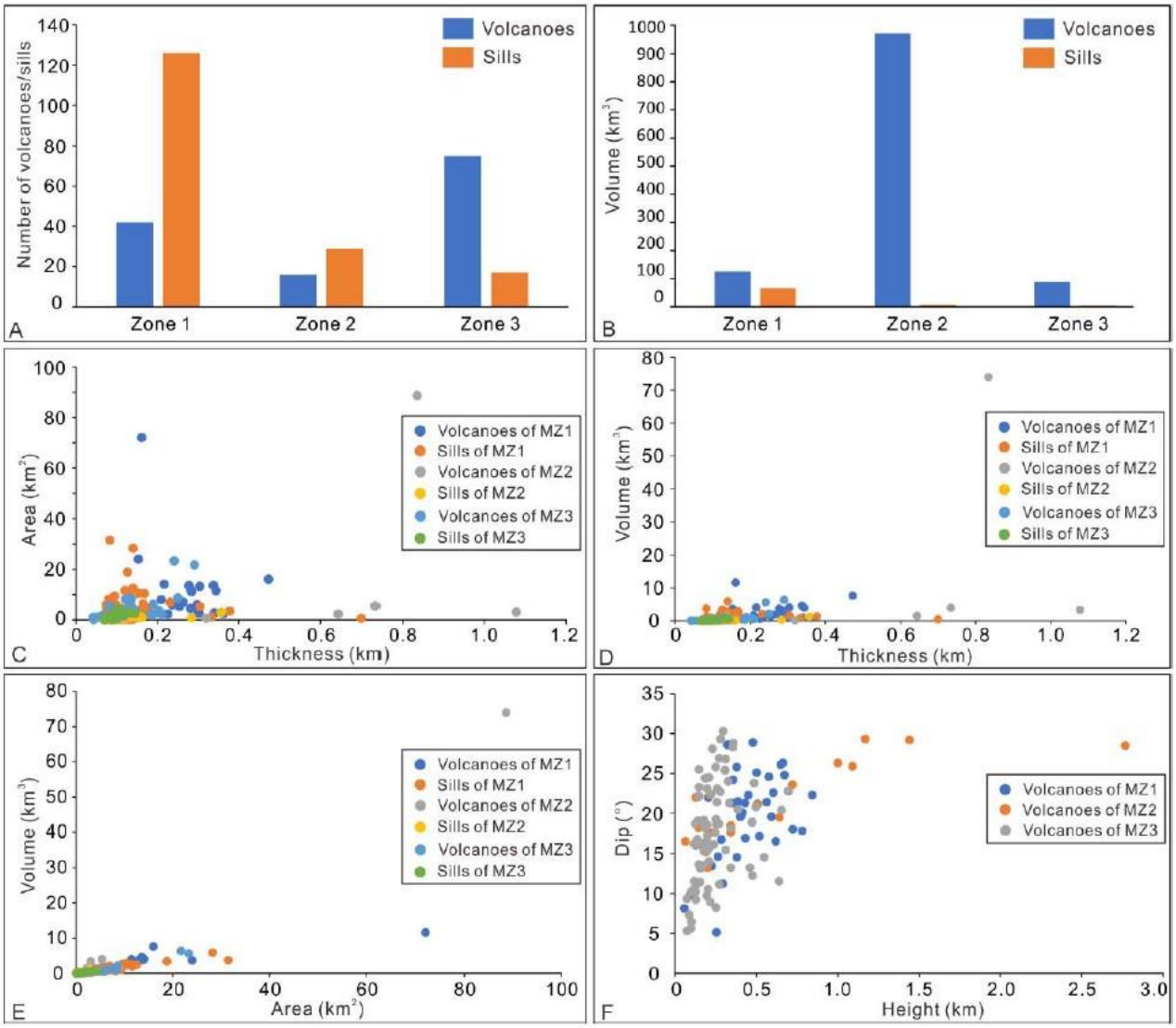

Figure 13: Dimensions of volcanoes and sills in zones MZ1 to MZ3. A: Number of volcanoes and sills; B: Volume of volcanoes and sills. C: Thickness vs. area of volcanoes and sills; D: Thickness vs. volume of volcanoes and sills. E: Area vs volume of volcanoes and sills. F: Height of volcanoes vs. flank gradient. Note that area and volume represent average values for the volcanic complex, e.g., area/volume of complex divided by number of volcanos in the complex.

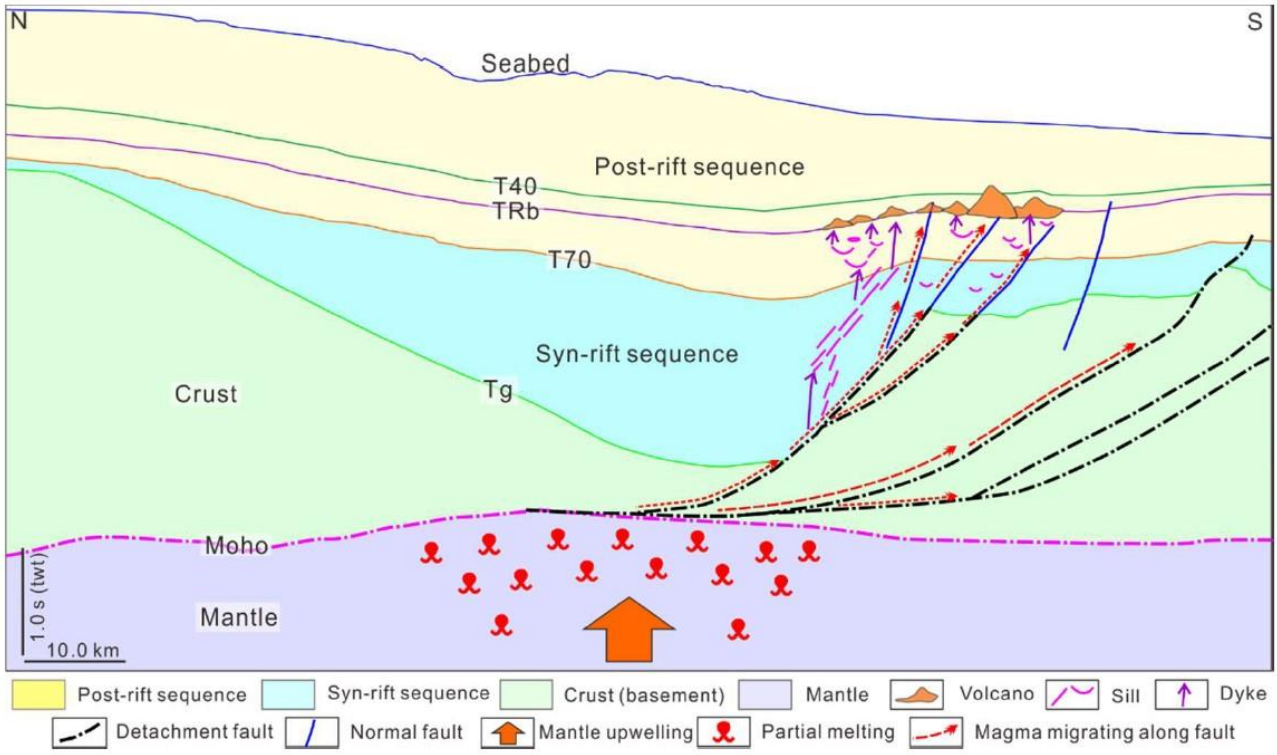

Figure 14: Model explaining the magma-migration mechanism from deep source areas to the early Miocene paleo-seabed. Magma used listric boundary faults to intrude the overlying strata - forming dikes and sills – or was extruded on the paleo-seabed as lava flows.

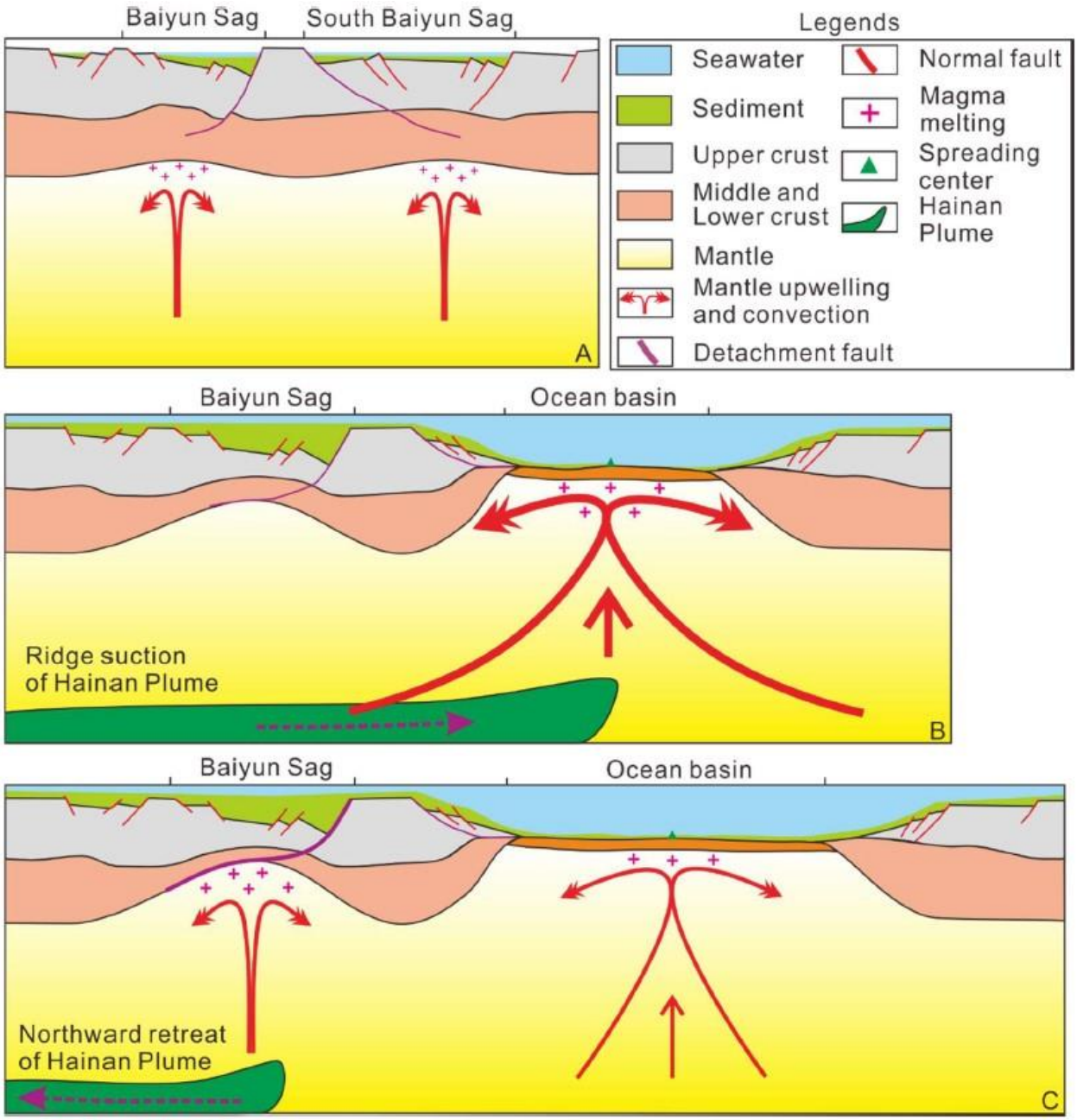

Figure 15: Magmatic sources in the Baiyun Sag. A: Graben/half-graben basins (sags) develop during the continental rifting of the South China Sea, with mantle upwelling occurring below the sags. Note that other sags in the northern SCS (e.g. Liwan Sag) are ignored in this model to better highlight the southern part of the Baiyun Sag as the locus of continental breakup. B: Continental breakup occurs in the southern part of the Baiyun Sag and mantle advection predominates in the spreading centre. A ridge suction effect forced the Hainan Plume to move towards the spreading centre. Mantle upwelling stopped below the Baiyun Sag at this stage. C: Seafloor spreading becomes weak and the Hainan Plume retreats northwards. The presence of the Hainan Plume and asscoiated adjustments caused the reactivation of mantle upwelling below the Baiyun Sag. This event triggered the intense and voluminous magmatism recognized in this work.

Table caption

Table S1: Dimensions, shapes and ages of volcanoes, sills and lava flows in the study area. Symbol '†' represents the magmatic edifices mapped in 2D seismic data. Symbol '∗' represents the magmatic edifices only mapped in one 2D seismic line - their areas and volumes are calculated approaching the magmatic edifices to the shape of a cylinder. Symbol '‡' indicate speculative ages of magmatic edifices based on the magmatic features around them. The shapes of volcanoes and lava flows are based on their plan-view. The shapes of sills are those observed on the seismic profiles. The areas of saucer and oblique sills are their plan-view projections. Volcano height is measured from the base of their edifices, rather than from the bases of eruptive materials. The plan-view shapes of volcanoes/lava flows and vertical sections of sills are also shown.